Energy Management Strategies for Hybrid Marine Powertrains

Siddharth Sasidharan

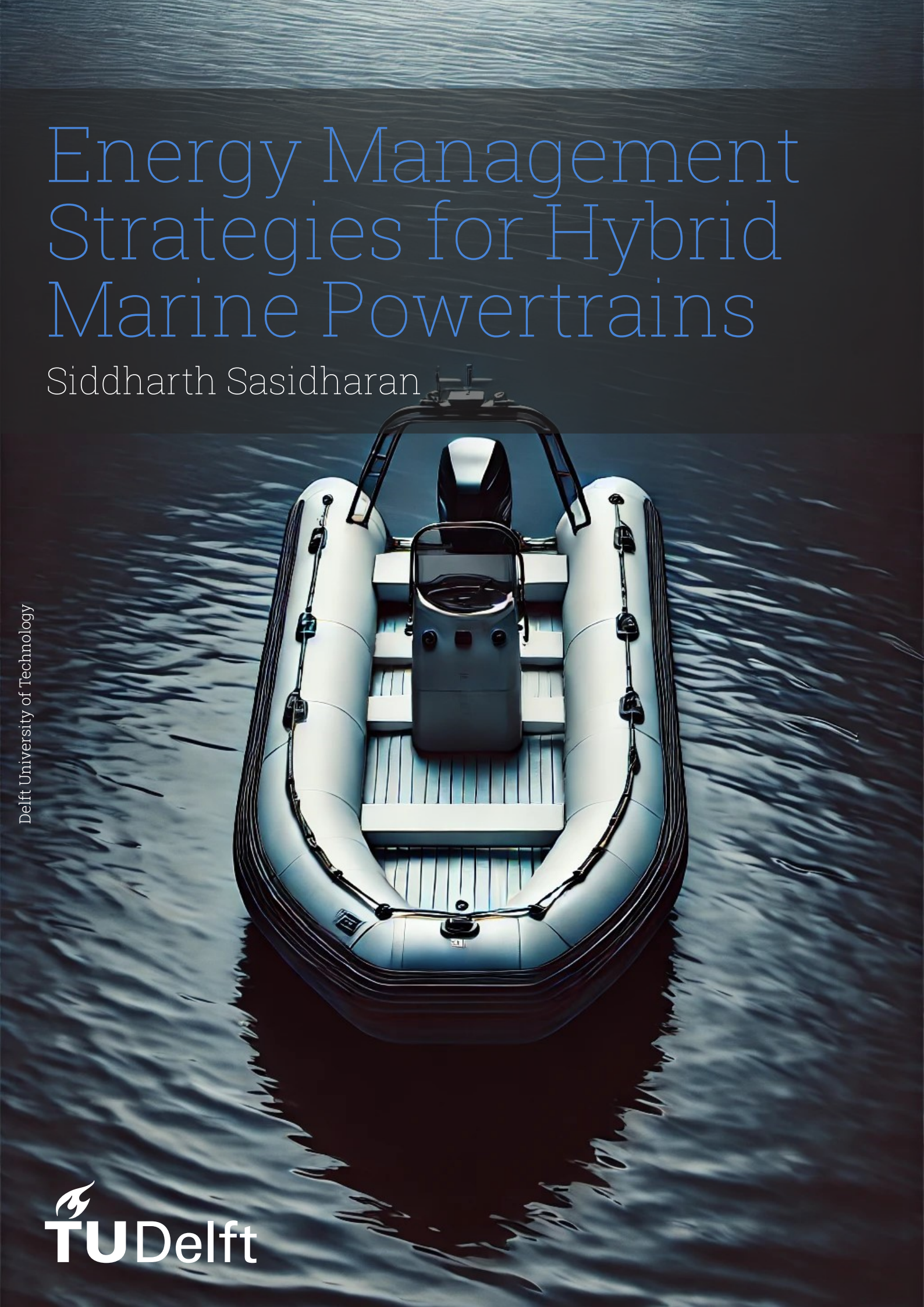

Delft University of Technology

TU Delft

Energy Management Strategies for Hybrid Marine Powertrains

by

Siddharth Sasidharan

Master Thesis

in partial fulfilment of the requirements for the degree of

Master of Science
in Mechanical Engineering

at the Department Maritime and Transport Technology of Faculty Mechanical Engineering of
Delft University of Technology
to be defended publicly on Monday October 21, 2024 at 14.00 hours

Student Number:	5788919
Track:	Multi-Machine Engineering
Report number:	MT.24/25.010.M

Supervisor:	Dr. Andrea Coraddu	
Thesis committee:	Dr. A. Coraddu (Chair)	Ship Design, Productions and Operations, ME
	Dr. V. Reppa	Transport Engineering and Logistics, ME
	Dr. L. van Biert	Ship Design, Productions and Operations, ME

Date: Friday 11th October, 2024

An electronic version of this thesis is available at http://repository.tudelft.nl/

Cover image of rigid inflatable boat generated at https://chat.openai.com/

TU Delft

Acknowledgements

I would like to express my deepest appreciation and gratitude to Dr. Andrea Coraddu for making this project possible. His support and insightful academic discussions have greatly contributed to the depth and quality of the work presented in this thesis. I would also like to extend my sincere thanks to Ege Ceyhun and Sofia Mendoza Contreras for their valuable guidance along the way. Furthermore, I am grateful to my friends for the countless brainstorming sessions, and for the wonderful memories shared over the past two years. Lastly, I would like to thank my family for their unwavering support throughout my entire academic journey.

Summary

Reducing carbon emissions and greenhouse gases in the transportation sector is crucial, given its significant contribution to environmental degradation. While fossil fuel-based machinery has been perfected over the past century, efforts towards improving hybrid electric and fully electric powertrains is promising in addressing the environmental challenges. For hybrid powertrains, achieving greener transportation involves developing efficient energy management strategies to distribute operational time and load between the system's multiple power sources. Among real-time strategies, optimization-based approaches have proven highly effective in minimizing energy consumption for specific scenarios. In particular, hierarchical optimization, with a focus on Model Predictive Control, has emerged as a logical and promising solution based on the existing literature.

Three control strategies were created in this study to be tested on a power plant modelled based on the H2C boat. The boat has a hybrid powertrain with a parallel architecture, powered by a low-temperature proton exchange membrane fuel cells and lithium ion batteries, rated at 50kW and 55kW respectively. The two power sources were mathematically modelled to balance computational simplicity with sufficient accuracy, closely reflecting the actual system. The study implemented three control strategies: a rule-based control, an offline optimization-based strategy, and Hierarchical Model Predictive Control (HMPC). They were evaluated based on their hydrogen consumption over the operational cycle, which was used as the key performance indicator (KPI). The rule-based control served as the upper bound for hydrogen consumption, while the offline optimization strategy, using Quadratic Programming, provided a benchmark for the lowest hydrogen consumption. This allowed for a comprehensive comparison to assess the competence of the Hierarchical MPC.

All three controls were designed with key considerations: maintaining the battery's state of charge within a safe and controllable range, meeting power demand as much as possible, and minimizing fuel cell power fluctuations while allowing the battery to handle transient changes. The objective of the Quadratic Programming (QP) problem was to minimize fuel cell power throughout the drive cycle and keep the fuel cell operating as close to its highest efficiency point as possible when active. The Hierarchical MPC's mathematical formulation was inspired by the Quadratic Programming approach. The HMPC consisted of two levels of optimization. The upper level computed the global optimal solution based on predicted power demand profiles, considering future operational plans, and passed it on to the lower level to be used as reference variables. The lower level featured an MPC that operated in real-time, managing disturbances in power demand to address the actual power profile. The objectives of the MPC were minimizing fuel cell power and the squared error between instantaneous fuel cell power and its highest efficiency point, similar to the QP problem. Additionally, it tracked the reference state from the upper level to bring the solution closer to global optimality.

The results showed that the Hierarchical MPC outperforms the rule-based control in all scenarios, while achieving performance close to the global optimal solution provided by the Quadratic Programming problem in terms of the KPI. Additionally, it showed strong results in reference tracking, reinforcing the effectiveness of the multi-level strategy and the information flow between the levels in improving real-time control. While further research is necessary to adapt the control strategy for real-world implementation due to the simplifications made during this study, the structure of the novel control strategy has proven to be highly competent.

In summary, this research presents a real-time control strategy that performs exceptionally well in systems where partial knowledge of a marine vessel's future operation is available. The basic framework introduced here can be further scaled to develop more accurate control strategies, capable of addressing additional objectives such as minimizing component degradation alongside energy management.

Contents

Acknowledgements i

Summary ii

1 Introduction 1

2 Literature Review 3
- 2.1 Energy Management Systems . . . 3
- 2.2 Offline EMS . . . 3
- 2.3 Real-time EMS . . . 4
  - 2.3.1 Rule-based EMS . . . 4
  - 2.3.2 Online Optimization-based EMS . . . 4
  - 2.3.3 Learning-based EMS . . . 5
- 2.4 Discussion . . . 5

3 Methodology 6
- 3.1 Plant Description . . . 6
- 3.2 Plant Modelling . . . 8
  - 3.2.1 Fuel cell . . . 8
  - 3.2.2 Battery . . . 11
- 3.3 State-Space Model . . . 12
- 3.4 Control Strategies . . . 13

4 Energy Management Strategies 14
- 4.1 Rule-based Control . . . 14
- 4.2 Quadratic Programming . . . 16
- 4.3 Hierarchical Model Predictive Control . . . 17

5 Results 19
- 5.1 Parameter Tuning for QP and HMPC . . . 19
- 5.2 Constraint Feasibility Check . . . 21
- 5.3 Robustness Check . . . 25
- 5.4 Control Strategy Comparison . . . 29

6 Conclusion 33

7 Recommendations and Future Work 35

List of Figures

3.1 H2C boat. Photo by Nikos Vasilikis. 6
3.2 Powertrain architecture of the boat 7
3.3 Operational profiles of the H2C boat 7
3.4 Detailed fuel cell stack model replicating the work of [1] 9
3.5 Determining output power of fuel cells 10
3.6 Rint equivalent circuit model 11

4.1 Flow chart for the Rule-based control 15
4.2 Hierarchical MPC 17

5.1 Grid search for ω determination in QP 20
5.2 Grid search for ω determination in HMPC 20
5.3 Test for N_p determination 21
5.4 Verification Test 1 22
5.5 Verification Test 2 23
5.6 Verification Test 3 - P_{fc} 24
5.7 Verification Test 3 - P_{bat} 25
5.8 Control Diagram 26
5.9 Test 1 for u_{fc} 27
5.10 Test 1 for P_{dem} 28
5.11 Test 1 for P_d 28
5.12 Test 2 for u_{fc} 28
5.13 Test 2 for P_{dem} 29
5.14 Test 2 for P_d 29
5.15 Quadratic Programming 30
5.16 Hierarchical MPC 31
5.17 Rule-based control 31

List of Tables

4.1 Rule-based control 15

5.1 Values of transfer functions 27
5.2 Control strategy comparison 32

Nomenclature

DP	Dynamic programming
ECMS	Equivalent consumption minimization strategy
EMS	Energy Management System
GHG	Greenhouse gas
HMPC	Hierarchical Model Predictive Control
IMO	International Maritime Organization
KPI	Key performance indicator
LP	Linear programming
MPC	Model Predictive Control
PEMFC	Proton-exchange membrane fuel cell
PMP	Pontryagin minimum principle
QP	Quadratic programming
RB	Rule-based control
RIB	Rigid-hull inflatable boat
RL	Reinforcement learning
SoC	State of Charge
WMO	World Metereological Organization

1

Introduction

The study of energy resources and climate change is critical to building a sustainable future. According to the World Meteorological Organization (WMO) [2], a specialized agency of the United Nations, 2023 has officially been recorded as the warmest year on record, with the average global temperature rising by 1.45 ° C above preindustrial levels. In addition to that, concentrations of the three main greenhouse gases, carbon dioxide, methane, and nitrous oxide, have increased to unprecedented levels. Given these alarming trends, there is a need to shift from fossil fuels to renewable energy sources. This transition is the key to reducing the adverse impacts of climate change.

The transportation sector contributes approximately 30 % to the total global greenhouse gas (GHG) emissions [3]. Recognizing this issue, the International Maritime Organization (IMO) has proposed a strategic plan aimed at achieving a 40 % reduction in GHG emissions by 2030 and a net-zero emission target by 2050 in the maritime sector [4]. Countries leading this effort include the EU, USA, Japan, China, and Korea. To enforce these targets, the IMO has implemented MARPOL regulations [5], which set strict limits on emissions from the engines of marine vessels. It is important to note that these regulations focus mainly on emissions rather than the power consumption of marine vessels [6].

The first step toward meeting these targets is the development and implementation of energy-efficient systems that can effectively manage both power consumption and emissions, while also addressing the challenges posed by the transition of the transportation sector to sustainability. Although electric and hybrid propulsion technologies hold great promise, significant obstacles remain, especially in improving fuel efficiency, optimizing energy storage systems, and perfecting the energy conversion processes between mechanical and electrical subsystems.

Fuel cell-powered hybrid powertrains have emerged as a good alternative, which couples electric propulsion driven by a fuel-cell system with an auxiliary battery. This configuration not only leads to reductions in emissions, but also minimizes environmental impact, with water and heat being the primary by-products of the propulsion process. The auxiliary battery plays a crucial role in ensuring adequate power delivery. Its charging and discharging cycles are closely related to the overall powertrain architecture and charge-sustenance characteristics.

Hybrid powertrain architectures vary depending on how energy contributions from different sources are managed. Passive architectures rely mainly on intermittent switching between power sources, whereas active systems use advanced energy management strategies to dynamically distribute and manage power across available sources [7]. Passive systems often face challenges related to system sizing and control, occasionally breaching safe operating limits and risking potential system breakdowns. As a result, active systems, which optimize the energy management, have become the focus of attention. Energy Management Systems (EMS) tailored to specific powertrain architecture, power sources, and energy storage systems are critical to maintaining system variables within predefined safety thresholds, thereby preventing catastrophic failures and enhancing overall performance. Addressing these challenges often requires the formulation and implementation of optimal control strategies tailored to

specific applications and configurations, which can improve the efficiency and reliability of hybrid systems.

Research efforts focused on optimizing strategies for energy management, system sizing and control, and trajectory planning, can offer insights into reducing emissions. By prioritizing innovation in these areas, the maritime sector can move closer to achieving its new regulations. This study focused on identifying and evaluating the capabilities of 3 different control strategies for energy management, specifically designed to minimize the fuel consumption of marine vessels. The three types of strategies explored are rule-based control, global optimization, and online optimization-based methods. A novel online optimization-based strategy, refered to as Hierarchical MPC was created for the system. The global optimization strategy was Quadratic Programming. The primary focus of this thesis was therefore, answering the following research question:

"How efficiently can a Hierarchical MPC perform in real-time for the energy management of a hybrid marine powertrain?"

To investigate this, the Rule-based control and Quadratic programming strategies were developed first. The Hierarchical Model Predictive Control (HMPC) strategy was created using an approach similar to Quadratic programming. Finally, the performance of the Hierarchical MPC was compared with the other two control strategies to assess its effectiveness in real-time energy management. This was done by looking into the following sub-questions:

- Is the solution given by the Hierarchical MPC more optimal than that provided by the Rule-based control?
- How close is the solution of the Hierarchical MPC to the global optimal solution?

Through these questions, the thesis aimed to assess the competence of Hierarchical Model Predictive Control strategy for the energy management of marine hybrid powertrains.

In this report, Chapter 2 provides an overview of the state-of-the-art energy management strategies that currently exist in the field and offers a brief background on how the concept for this research originated. Chapter 3 details the methodology, including the modelling of the powerplant and the specifications of the marine vessel used in the study. Chapter 4 explains the three Energy Management Strategies, discussing each in detail and covering the mathematical formulations for the optimization problems as well as the rules governing the rule-based control strategy. Chapter 5 presents the results, observations, and answers to the research questions. It includes a comparison of the strategies using fuel consumption as the key performance indicator, along with constraint feasibility and robustness tests.

2

Literature Review

This chapter introduces the different energy management systems available in the literature, focusing primarily on the control strategies for hybrid powertrains in the automotive, marine and aviation industries. The literature gap, the need for efficient control, and the basis for their formulation are discussed.

2.1. Energy Management Systems

Energy Management Systems regulate the power distribution among the various components of a powertrain by carefully modeling powertrain dynamics and establishing relationships that define power flow. While the primary objective of most EMSs is to minimize fuel consumption, these strategies often encompass additional goals, such as optimizing the sizing of key powertrain components, mitigating battery degradation, and reducing pollutants and emissions.

EMSs are typically classified into two main categories: offline and real-time. A common sub-classification for real-time EMSs includes rule-based, optimization-based, and learning-based strategies [8]. The following sections provide an overview of these EMS classifications, their operational mechanisms, and discusses the scenarios in which each method is most effective.

2.2. Offline EMS

Strategies which optimize energy management using prior knowledge of the drive cycle and relevant energy variables' trajectories (such as speed, torque or power) are classified as Offline strategies. These include Dynamic programming (DP), Pontryagin Minimum Principle (PMP), Linear Programming (LP), Quadratic Programming (QP) and Convex Programming. Offline strategies can be further categorized based on their applications: they may serve as benchmarks, form part of a multi-level EMS, or act as the foundation for online EMS development.

- Benchmark: The work of Li et al. [9] illustrates how offline strategies, such as Dynamic Programming (DP), are used as benchmarks to evaluate the performance of real-time strategies. Due to the availability of prior knowledge, offline strategies provide globally optimized solutions, offering the best possible outcome for a given situation. This helps in using it as a benchmark for comparing other control strategies. A variant of DP, known as Stochastic Dynamic Programming, is employed by Moura et al. [10] and Johannesson et al. [11] for comparison with other strategies. Other offline optimization methods, such as the Mixed-Integer Optimal Control Problem [12], Convex Optimization [13], and Slope-weighted Energy-based Rapid Control Analysis (SERCA) [14], are also used as benchmarks. The choice of an offline optimization strategy depends on factors such as the specifications of the plant being controlled, the computational complexity, and the acceptable error tolerance in the optimization process.
- Part of Multi-level EMS: The offline strategies have often been used as the part of a bigger system.

It acts as an optimizer at the cloud level, providing information and data for a real-time control at the lower level. The computational complexity of the global optimization being an issue for working in real time is surpassed by having it in the cloud level, taking its time to run the optimization, and finally providing the guidance for the real-time strategy to arrive at better solutions. Often, for managing multiple vehicles together in a system, this layered architecture is used for cloud-to-vehicle connectivity [15]. For energy management in a single vehicle, a two-layer EMS can be used where the first layer that utilizes an offline optimization-based strategy, makes the day-ahead energy dispatching plans with minimal fuel consumption [16].

- Base for online EMS: The offline optimizers are often used as a foundation for developing real-time strategies. For example, an offline control strategy based on Pontryagin's Minimum Principle [17] is used to develop the Equivalent Consumption Minimization Strategy (ECMS), which functions as a real-time control. Similarly, a Dynamic Programming-based EMS for a fuel-cell/battery hybrid energy storage system has been proposed and implemented as a real-time solution [18].

As stated above,offline strategies can deliver a global optimum for any feasible optimization problem. However, their limitation lies in the inability to provide solutions in real-time.

2.3. Real-time EMS

Real-time strategies are characterized by their simplicity, reduced computation time, predictive capabilities, and instantaneous implementation. These strategies can be broadly classified into three categories: rule-based, online optimization-based, and learning-based control strategies.

2.3.1. Rule-based EMS

These strategies are based on pre-calculated rules, that cannot be altered or reprogrammed during operation without human intervention [19]. They may use deterministic or fuzzy rules, or utilize look-up tables. Owing to their simplicity, Rule-based (RB) EMSs can be implemented in real-time. However, they have several drawbacks, the most significant being their inability to provide optimal solutions. The calibration effort required to guarantee satisfactory performance is high, and the rules are not scalable to accommodate different powertrain architectures or different component sizes [8].

RB EMSs can be further categorized into Deterministic and Fuzzy logic control strategies. A deterministic RB-EMS operates on predetermined rules derived from experience. The control strategy is designed to make the power system operate in regions of minimal energy consumption, high efficiency power-torque delivery, minimal energy transmission losses, or achieving an overall optimal operational point.

Fuzzy Logic Control on the other hand can be considered as an extension of binary logic, where instead of a strict ON-OFF criteria or a binary (1 and 0) value, multiple values or fuzzy partition of the inputs are considered. An input-output relation is established in each fuzzy subspace. Fuzzy logic consists of three stages; fuzzification, rule-base system and defuzzification process. There are two types of Fuzzy methods; Mamdani type and Takagi-Sugeno-Kang (TSK) type. In the TSK fuzzy logic [20], the model assumes the form, *"If SoC is High and P_{load} is high, C = y (SoC, P_{load})"* where y represents a variable of consequence whose value is inferred from the variables of premise, SoC and P_{load}. Mamdani fuzzy logic method regards the output as a fuzzy partition, much like the input variables. Outputs can be tabulated relative to the input values for each of their combinations. The strategies used by the fuzzy logic controls in [21] and [22], and the fuzzy component of the Fuzzy state machine (FSM) strategy in [23] use Mamdani's fuzzy inference approach.

2.3.2. Online Optimization-based EMS

Optimization-based strategies which can be implemented online are characterized by their causal nature, local optimization, and independence from prior knowledge of the drive cycle. In real-time optimization methods, the control variable is determined by minimising a predefined cost function based on future equivalence assumption of the electric energy consumption [24]. The most widely used strategies

in this category are ECMS (Equivalent Consumption Minimisation Strategy) and MPC (Model Predictive Control).

ECMS operates on the principles of static optimization, wherein the cost function that consists of engine and battery-related costs, is minimised instantaneously. The power demand need not be known in advance, which therefore enables real-time application. PMP is reformulated into a local optimisation problem to obtain ECMS, by minimising the equivalence factor, analogous to the role of costate in PMP. The equivalence factor accounts for the fuel consumption for battery recharging and regenerative braking energy [8]. Diniz et al.[25] proposes an enhanced version of this technique, called Adaptive-ECMS (A-ECMS), where a variable equivalence factor is defined by a battery penalty factor, which is dependant on the battery SoC range and charging/discharging efficiency.

Model Predictive Control determines the local optimal solution through prediction over a specified horizon. It has widespread applications, ranging from Robotics to Supply chains. Based on the initial inputs at a given instant, it computes the inputs over a predictive horizon to minimise the objective function subject to constraints. However, only the first set of inputs in the immediate time step is executed. The prediction horizon then progresses forward to the next time step, and the process is repeated until the end [26]. MPC is capable of handling multivariable processes, managing extended time delays, and integrating disturbance response knowledge [27].

In addition to classic ECMS and MPC, there are variations such as dual-state adaptive ECMS and double-layer fuzzy adaptive nonlinear MPC, as well as other real-time optimization strategies like transient process optimization control [28].

2.3.3. Learning-based EMS

In a Learning-based EMS, the necessity for precise model information diminishes, as control decisions are made based on learning through interactions with the environment. A reinforcement learning (RL) system consists of a learning agent and studies its interaction with the environment. At each time step, the learning agent receives an observation of the environment, selects an action based on the observed state, transitions to a new state as a result of the action, and then computes the reward associated with the transition. This reward is then provided as a feedback to the learning agent. Over time, through the iterative process, the optimal policy can guide the learning agent to take the best series of actions to maximise the cumulated reward.

Variations of the reinforcement learning method can be seen in the works of Hu et al.[29] and Gao et al.[30], who utilize deep RL and safe RL methods, respectively.

2.4. Discussion

This chapter leads to several key conclusions. First, the inability of rule-based control strategies to provide optimal solution means they can serve as an upper bound of minimization control problems for real-time strategies, which should not be easily surpassed. Second, offline optimization strategies can serve both as benchmarks for real-time strategies and as foundational elements for their development. Third, combining various strategies, each focusing on its unique strengths, may offer the most effective approach in terms of creating a control strategy. A well-balanced mix of strategies to address specific objectives, such as fuel consumption, emissions, and battery degradation could lead to optimal performance. In this regard, a Model Predictive Control (MPC) operating in a hierarchical manner appears promising. These three findings from the literature have been used in this research to come up with a good hierarchical MPC strategy and a process to compare and assess its capabilities, which are detailed later in this thesis.

3

Methodology

In this chapter, the specifications of the boat for which the EMSs are created are described in section 3.1. This is followed by a description of the mathematical modelling of the hybrid powertrain of the boat in section 3.2. Based on plant modelling, powertrain architecture and power balance relations, the state-space equations are then formulated in section 3.3.

3.1. Plant Description

The marine vessel utilized in this research is an H2C boat, a hydrogen-powered rigid-hull inflatable boat (RIB or RHIB) with a hull made of either polyester or aluminium [31]. Such boats are typically equipped with powerful onboard engines. This particular vessel is powered by hydrogen fuel cells and lithium-ion batteries.

Figure 3.1: H2C boat. Photo by Nikos Vasilikis.

The powertrain architecture of the boat is illustrated in Figure 3.2. It is a parallel configuration with a unidirectional flow of energy from the fuel cell to the DC converters and a bidirectional flow for the battery, to accommodate charging and discharging of the Lithium-ion batteries. The DC converters are

connected to the DC bus and then to a motor which propels the boat forward. Regenerative braking is not considered in this study.

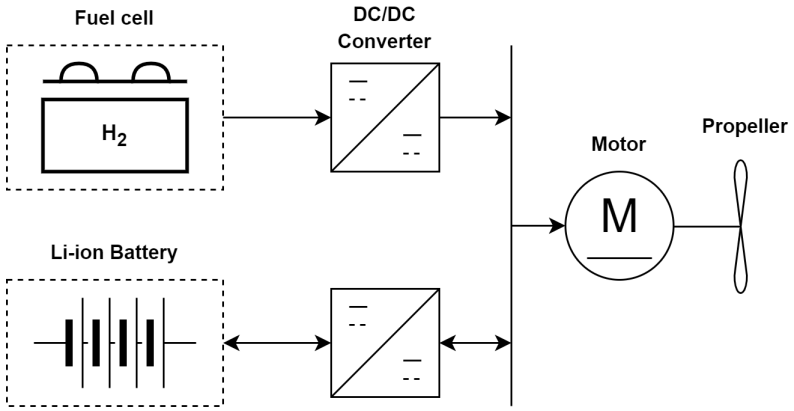

Figure 3.2: Powertrain architecture of the boat

A 'Deep Blue' electric drive system from the company Torqeedo [32] is used on the boat. The Lithium-ion battery has a usable capacity of 38 kWh with a 2 kWh reserve, a nominal voltage of 360 V, and can deliver a continuous maximum power of 55 kW. Fuel cell serves as a range extender. Although specific details of the fuel cell and hydrogen storage are not available, it is known that a low-temperature proton-exchange membrane fuel cell (LT-PEMFC) is used. For the purposes of this research, it is assumed that the fuel cell can deliver a maximum power of 50 kW and that the hydrogen storage has unlimited capacity. Due to time constraints and the specific focus of the optimization strategies on the power-split between sources, the propulsion motor and DC-DC converters have been excluded from the plant model.

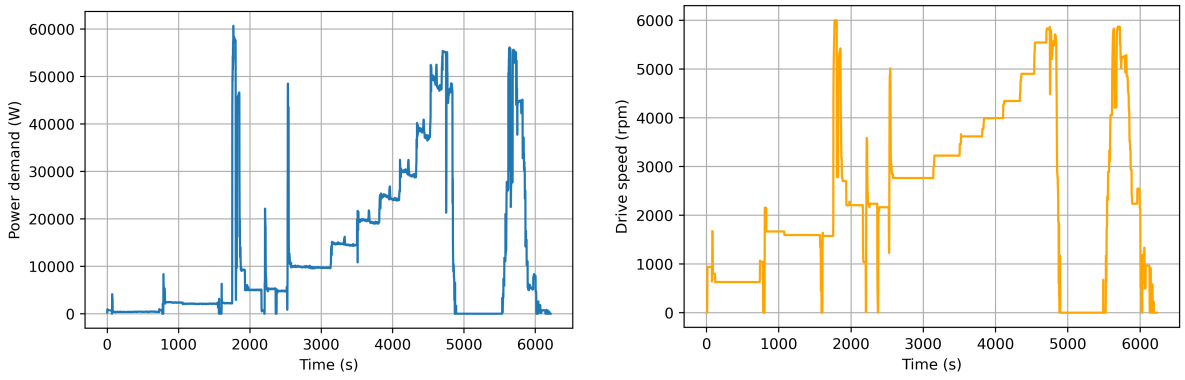

(a) Power profile

(b) Motor speed profile

Figure 3.3: Operational profiles of the H2C boat

The profiles in Figure 3.3 are based on real data retrieved from the boat's operations. Figure 3.3b shows the speed of the motor in the boat's powertrain over the time period. The profile illustrated in Figure 3.3a is the fundamental drive cycle data with a maximum power demand of 60.91 kW, from which most of the power profiles for the experiments were created. Disturbances in power were introduced to the profile as a stochastic variable with a limited rate of change, simulating uncertainties typically encountered in real-world conditions. Since this research focuses on the power balance and power-split among the components, drive cycle data other than power profiles were not considered for experimentation.

3.2. Plant Modelling

3.2.1. Fuel cell

Fuel cells are electrochemical devices which convert energy from chemical reactions into electrical energy. They can be categorised based on the type of fuel being used and the operational temperatures. The main types include alkaline fuel cells (AFC), solid oxide fuel cells (SOFC), phosphoric acid fuel cells (PAFC), molten carbonate fuel cells (MCFC) and proton-exchange membrane fuel cells (PEMFC). For the system in question, a low-temperature PEMFC is used aboard the boat. A PEMFC offers several superior features over the others, like low operating temperatures, fast start-up, high power density, long lifespan and minimal corrosion.

The PEM fuel cell is made up of two electrodes coated with a platinum catalyst, separated by a proton exchange membrane. During operation, humidified hydrogen or a hydrocarbon-based fuel enters the anode side of the fuel cell, while an oxygen stream enters the cathode side [33]. At the anode, the fuel is oxidized in the presence of the catalyst, producing H^+ ions and releasing electrons. These electrons travel through an external circuit to the cathode. Meanwhile, the proton exchange membrane allows only the positively charged hydrogen ions (protons) to pass from the anode to the cathode [34].

The electrochemical reactions are as follows:

at anode:

$$2H_2 \rightarrow 4H^+ + 4e^- \tag{3.1}$$

at cathode:

$$O_2 + 4H^+ + 4e^- \rightarrow 2H_2O \tag{3.2}$$

overall reaction:

$$2H_2 + O_2 \rightarrow 2H_2O \tag{3.3}$$

The reaction in addition to producing electricity, is exothermic in nature. For one cell, the reversible electric potential is calculated as follows:

$$E_{cell} = -\frac{\Delta G}{zF} \tag{3.4}$$

where ΔG is the change in Gibb's free energy and F (96485.33 C/mol) is Faraday's constant, which is computed as the product of elementary charge (in coulombs) and the Avagadro's constant. z is the number of moving electrons or the number of electrons released by each molecule of hydrogen (z = 2). The maximum electrical work done by a fuel cell at constant temperature and pressure is given by the change in Gibb's free energy. This can also be given as follows:

$$\Delta G = \Delta G_0 - RT \ln \left[\frac{P_{H_2} \cdot (P_{O_2})^{0.5}}{P_{H_2O}} \right] \tag{3.5}$$

where ΔG_0 change in Gibb's free energy at standard operating conditions, R is the universal gas constant, T is the stack temperature, and P_{H_2}, P_{O_2} and P_{H_2O} are the partial pressures (in atm) of hydrogen, oxygen and water respectively. Upon substituting Equation 3.4 in Equation 3.5, Nernst potential of one cell is obtained as follows:

$$E_n = E_0 + RT \ln \left[\frac{P_{H_2} \cdot (P_{O_2})^{0.5}}{P_{H_2O}} \right] \tag{3.6}$$

The detailed fuel cell model is based on the works of Njoya et. al [1] and Xun et al. [35]. It considers parameters such as pressures, temperature, compositions, and flow rates of fuel and air. Considering the kinetics of the reactions, the fuel cell voltage can be given as follows:

$$V_{fc} = E_{oc} - V_{act} - I_{fc} R_{ohm} \tag{3.7}$$

$$E_{oc} = NK_cE_n \tag{3.8}$$

$$V_{act} = NA\ln\left[\frac{I_{fc}}{I_0}\right] \cdot \frac{1}{sT_d/3+1} \tag{3.9}$$

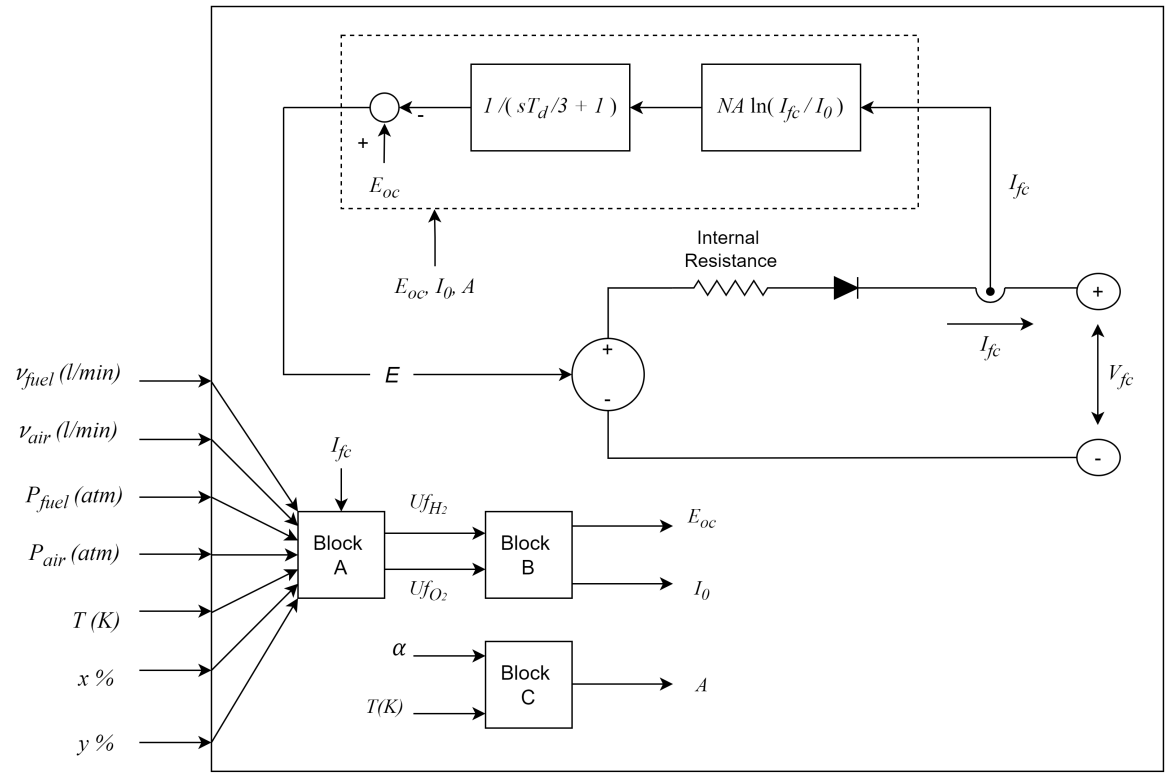

Figure 3.4: Detailed fuel cell stack model replicating the work of [1]

where E_{oc} is the open circuit voltage (V), V_{act} is the voltage due to activation losses (V), I_{fc} is the fuel cell current (A), R_{ohm} is the internal resistance (Ω), N is the number of cells, K_c is the voltage constant at nominal condition of operation, A is the Tafel slope (V), I_0 is the exchange current (A), and T_d is the stack settling time or response time (at 95% of the final value). The activation losses, which characterises the delayed response due to the rate of chemical reactions at the electrode surfaces, is represented by the first order transfer function $\frac{1}{sTd/3+1}$, with s being the frequency variable in the Laplace domain.

The model is illustrated in detail in the Figure 3.4. Using the blocks A, B and C, where E_{oc}, I_0 and A are updated based on the varying parameters ν_{fuel} (fuel flow rate in litres/min), ν_{air} (air flow rate in litres/min), P_{fuel} (absolute supply pressure of fuel in atm), P_{air} (absolute supply pressure of air in atm), T, $x\%$ (percentage of hydrogen in the fuel) and $y\%$ (percentage of oxygen in the oxidant) . Using these inputs into Block A, the rate of utilization of hydrogen and oxygen are calculated as follows:

$$Uf_{H_2} = \frac{60000RTI_{fc}}{zFP_{fuel}\nu_{fuel}x\%} \tag{3.10}$$

$$Uf_{O_2} = \frac{60000RTI_{fc}}{2zFP_{air}\nu_{air}y\%} \tag{3.11}$$

In the block B, to calculate the Nernst voltage and exchange current, the partial pressures are computed as follows:

$$P_{H_2} = (1 - Uf_{H_2})x\%P_{fuel} \tag{3.12}$$

$$P_{O_2} = (1 - Uf_{O_2})y\%P_{air} \tag{3.13}$$

$$P_{H_2O} = (w + 2y\%Uf_{O_2})P_{air} \tag{3.14}$$

In the Nernst equation, P_{H_2O} becomes 1 if T<373K. Finally, using the values of partial pressures and the Nernst voltage, block B and C computes I_0 and A as follows:

$$I_0 = \frac{zFk\left(P_{H_2} + P_{O_2}\right)}{Rh} \cdot \exp\left(\frac{-\Delta G}{RT}\right) \tag{3.15}$$

$$A = \frac{RT}{z\alpha F} \tag{3.16}$$

where k is the Boltzmann's constant (1.38×10^{-23} J/K) and h is the Planck's constant (6.626×10^{-34} Js).

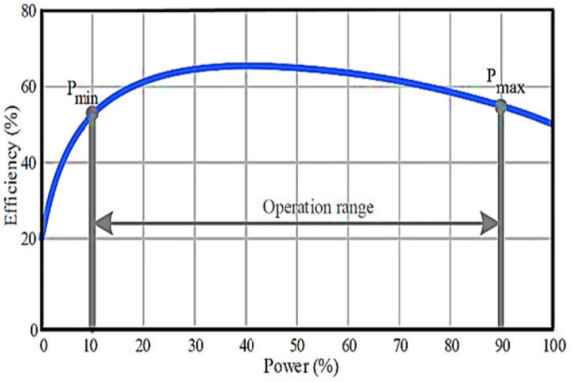

(a) Efficiency of fuel cells as given in [36]

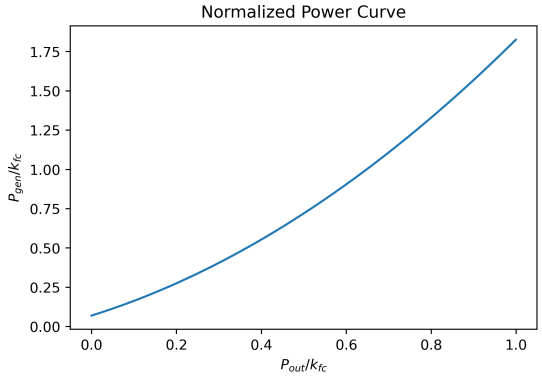

(b) Normalized generated power with respect to the output power of fuel cell systems

Figure 3.5: Determining output power of fuel cells

The energy management strategies are designed to optimize the power split between energy sources. While the fuel cell can provide reliable power at steady state conditions, some of the power it generates is wasted and cannot be delivered to the load due to activation losses, ohmic losses, mass transfer or concentration losses, and thermal losses. As illustrated in the Figure 3.5a [36], these losses vary with the power generated by the fuel cell. The efficiency is therefore dependent on the amount of power generated by it. Using the data from this graph, the relationship between the normalized values of generated power and the actual power output is established in the Figure 3.5b. The actual output power is the product of fuel cell's efficiency and generated power (denoted in Figure 3.5a as power(%)). By performing curve fitting, the normalized power curve can be defined as a quadratic function, given by:

$$\frac{P_{fc_{gen}}}{k_{fc}} = 0.9131 \cdot \left(\frac{P_{fc_{out}}}{k_{fc}}\right)^2 + 0.8451 \cdot \left(\frac{P_{fc_{out}}}{k_{fc}}\right) + 0.0700 \tag{3.17}$$

$$P_{fc_{gen}} = E_{oc} \cdot I_{fc} \tag{3.18}$$

where k_{fc} is the maximum rated power output of the fuel cell, considering all the losses.

The objective of the EMSs is to minimise the fuel consumption over the drive cycle. 1 kg of Hydrogen contains 33.33 kWh of usable energy. Thus, to calculate the instantaneous hydrogen consumption, the following relation is used:

$$m_{H_2}(t) = P_{fc_{gen}}(t) \cdot \Delta t \cdot \mu \tag{3.19}$$

where m_{H_2} (kg) is the mass of hydrogen consumed and μ (kg/kWh) is the reciprocal of usable energy of Hydrogen.

The following assumptions were made when the fuel cell model was designed by Njoya et. al [1]:

- The gases behave ideally.
- The cooling system in the fuel cell is able to manage the stack temperature which is assumed to be equal to the temperature at the cathode and anode.
- Water management system in the fuel cell is able to manage the humidity inside it at any load.
- The pressure drops across channels are negligible.
- The cell resistance is assumed to be constant even in varying temperature and humidity.
- Fluid flow through the membranes are not taken into account.

3.2.2. Battery

The second power source for the H2C boat is a Lithium-ion battery. These batteries are widely used in the automotive industry and for energy storage applications due to their electrochemical stability, high energy density, and long cycle life.

To accurately model the working characteristics of this battery, an equivalent circuit modelling concept is used. An equivalent circuit model uses a semi-mechanical and semi-empirical approach to describe the battery [37]. Commonly used models include the Rint and Thevenin models. While the Thevenin model accounts for the polarization effects of the lithium-ion battery and provides a more precise behavioural representation, this research utilizes the Rint model due to its computational simplicity and minimal-data approach.

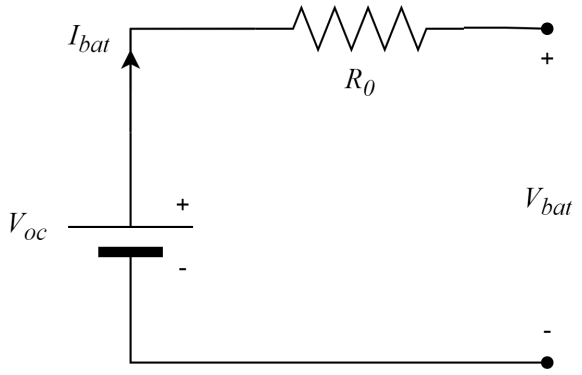

Figure 3.6: Rint equivalent circuit model

The Equivalent circuit consists of an ideal voltage source and a resistance R_0, as illustrated in the Figure 3.6. The resistance R_0 characterizes the internal ohmic resistance of the battery. Using Kirchoff's law, we obtain the relation:

$$V_{bat} = V_{oc} - I_{bat}R_0 \tag{3.20}$$

where V_{oc} is the battery's open circuit voltage (which assumed to be a constant) and I_{bat} is the current flowing through the circuit. The only loss in power in this scenario is due to the internal resistance. The power drawn and the power losses from the battery can thus be defined as follows:

$$P_{bat} = V_{oc}I_{bat} \tag{3.21}$$

$$P_{loss} = I_{bat}^2 R_0 \tag{3.22}$$

An important property of the battery on which its performance depends is the State of Charge (SoC). It is a unitless quantity which represents the remaining useful charge inside the battery and can be expressed as follows [38]:

$$SoC(t + \Delta t) = SoC(t) - \frac{P_{bat}(t) \cdot \Delta t}{E_{bat}} \tag{3.23}$$

where E_{bat} is the energy rating of the battery.

3.3. State-Space Model

The relationship between the models of fuel cell and battery created in the previous sections was established by a power balance equation 3.24 to represent the hybrid marine powertrain.

$$P_{dem} = P_{fc_{out}} + P_{bat} - P_{loss} \tag{3.24}$$

The relationship governing the power-split between the two power sources dictates that the power demand P_{dem} is met by the fuel cell output $P_{fc_{out}}$ and the battery power P_{bat} at every instant. If the battery is discharging, P_{bat} is positive and if charging, P_{bat} is negative. Referring again to Equation 3.24, this implies that during the battery's charging phase, both the power required for charging and the power demand are supplied by the fuel cell output.

Equation 3.23 was transformed into a state-space representation of the system in the discrete-time domain. The battery state of charge was chosen as the state variable, while the ratio of the fuel cell's power output at any given instant to the maximum output power of the fuel cell, referred to as normalized fuel cell power u_{fc} defined in Equation 3.28, served as the manipulated or control variable. To derive the state-space model, Equation 3.24 was substituted into Equation 3.23. This substitution resulted in the formulation of the following state-space model for the energy management system:

$$x(k+1) = Ax(k) + Bu(k) + Ed(k) \tag{3.25}$$

$$y(k) = Cx(k) + Du(k) + Fd(k) \tag{3.26}$$

where the state variable x denotes the state of charge, u denotes the input variables, and d represents the disturbances. Specifically for this system, the coefficients and the variables are defined as follows:

$$u(k) = \begin{bmatrix} u_{fc} \\ P_{dem} \end{bmatrix}, d(k) = \begin{bmatrix} P_{loss} \\ P_d \end{bmatrix},$$

$$A = 1, \quad B = \begin{bmatrix} \frac{k_{fc} \cdot \tau_s}{E_{bat}} & \frac{-\tau_s}{E_{bat}} \end{bmatrix}, \quad E = \begin{bmatrix} \frac{-\tau_s}{E_{bat}} & \frac{-\tau_s}{E_{bat}} \end{bmatrix}, \quad C = 1, \quad D = \begin{bmatrix} 0 & 0 \end{bmatrix}, \quad F = \begin{bmatrix} 0 & 0 \end{bmatrix}$$

This can be rewritten as:

$$SoC(k+1) = SoC(k) + \left[\frac{k_{fc} \cdot \tau_s}{E_{bat}}\right] u_{fc}(k) - \left[\frac{\tau_s}{E_{bat}}\right] P_{dem}(k) - \left[\frac{\tau_s}{E_{bat}}\right] P_{loss}(k) - \left[\frac{\tau_s}{E_{bat}}\right] P_d(k) \tag{3.27}$$

$$u_{fc}(k) = \frac{P_{fc_{out}}(k)}{k_{fc}} \tag{3.28}$$

where k_{fc} is the maximum output power of the fuel cell, u_{fc} is the normalized fuel cell power, E_{bat} is the energy rating of the battery, P_{dem} is the power demand which is considered as an exogenous input, P_{loss} is the power loss from the battery, P_d is any variations in the power demand, and τ_s is the sample time. Considering the power balance and battery dynamics alone, approaching the problem with minimal data, this single state-space equation is used to represent the system.

3.4. Control Strategies

In this research, three distinct control strategies were developed for managing energy and power distribution among the power sources of the H2C boat: Rule-Based (RB) Control, Global Optimization using Quadratic Programming (QP), and Hierarchical Model Predictive Control (HMPC). QP was chosen for its similarity to classical Model Predictive Control (MPC) in formulation and structure. The Rule-based control and HMPC works in real-time, while the QP is an offline control strategy. The RB and QP strategies were utilized to compare performance and assess the potential of the HMPC.

RB was designed based on predefined rules that do not adapt dynamically. It was anticipated that QP would provide the most optimized results, while RB would yield the least effective performance. Therefore, QP served as the benchmark, and RB represented the upper threshold of performance for HMPC.

The control strategies determined the amount of power to be produced by the fuel cell and the battery at any given moment during operation, with the goal of minimizing total hydrogen consumption over the power profile. They were set up in such a way that the battery handled fluctuations and transient power variations, while the fuel cell maintained a minimal rate of power change. This research did not address degradation mechanisms or the optimization of component sizing in the powertrain.

The rule-based control was designed and implemented using Matlab and Simulink. The quadratic programming problem and the HMPC was formulated in python using the 'Gurobi' package for optimization. The performance of these strategies were evaluated based on the KPI, the total hydrogen consumption over the entire drive cycle of a given power profile.

4

Energy Management Strategies

This chapter provides an overview of the energy management strategies and their mathematical formulations. It introduces three distinct control strategies, two of which are optimization-based. All three strategies are designed to adhere to the following core principles:

- Minimize hydrogen use
- When the fuel cell is in operation, maximize its efficiency, which inadvertently means operating the fuel cell at or near its optimal power output, P_{opt}. The optimal power of the fuel cell is illustrated in Figure 3.5a by the maximum value of the curve.
- Always meet the power demand.
- Maintain the battery SoC within limits. This helps with reducing battery degradation.
- Use battery to absorb sudden changes in power demand, while the fuel cell's power output should be kept as stable as possible.

4.1. Rule-based Control

As illustrated in Figure 4.1, the rule-based control was designed with three inputs and two outputs. It operates in the discrete time domain to avoid complications associated with an oscillating switch between charging and discharging modes of the battery. P_{bat}, the power consumed or delivered by the battery in the current time-step is used as an input to it. A negative value of P_{bat} indicates charging, and positive value indicates the discharging mode. The other two inputs are the power demand for the upcoming time-step and the battery state of charge of the current time-step. Determination of power-split between the fuel cell and battery, and whether or not they should be turned off at any point are decided by only these three inputs. The outputs are the fuel cell power and battery power requested for the next time-step. For simplicity, $P_{fc_{out}}$ is denoted as P_{fc} in this section.

The control strategy is created such that it strictly follows the following rules:

- Battery SoC is maintained in the range $[SoC_{min}, SoC_{max}]$.
- The fuel cell, if possible, operates at $P_{fc} = P_{opt}$
- The rate of change of P_{fc} is limited to $[-\epsilon, \epsilon]$ to enable smooth operation of the fuel cell.

The control first compares the battery SoC to its allowable range. If the SoC is within the range $[SoC_{min}, SoC_{max})$, it looks into whether the battery was charging or discharging at that instant, and then makes a decision considering the power demand. If the SoC is below SoC_{min}, the battery is charged unless the power demand is greater than the optimal power output of the fuel cell. However, if the SoC is greater than or equal to SoC_{max}, the power demand is satisfied by the battery alone, as long as it is below P_{opt}. If the demand is more, the power is split among the power sources.

Table 4.1 gives a detailed explanation of these rules and their implementation in the control strategy.

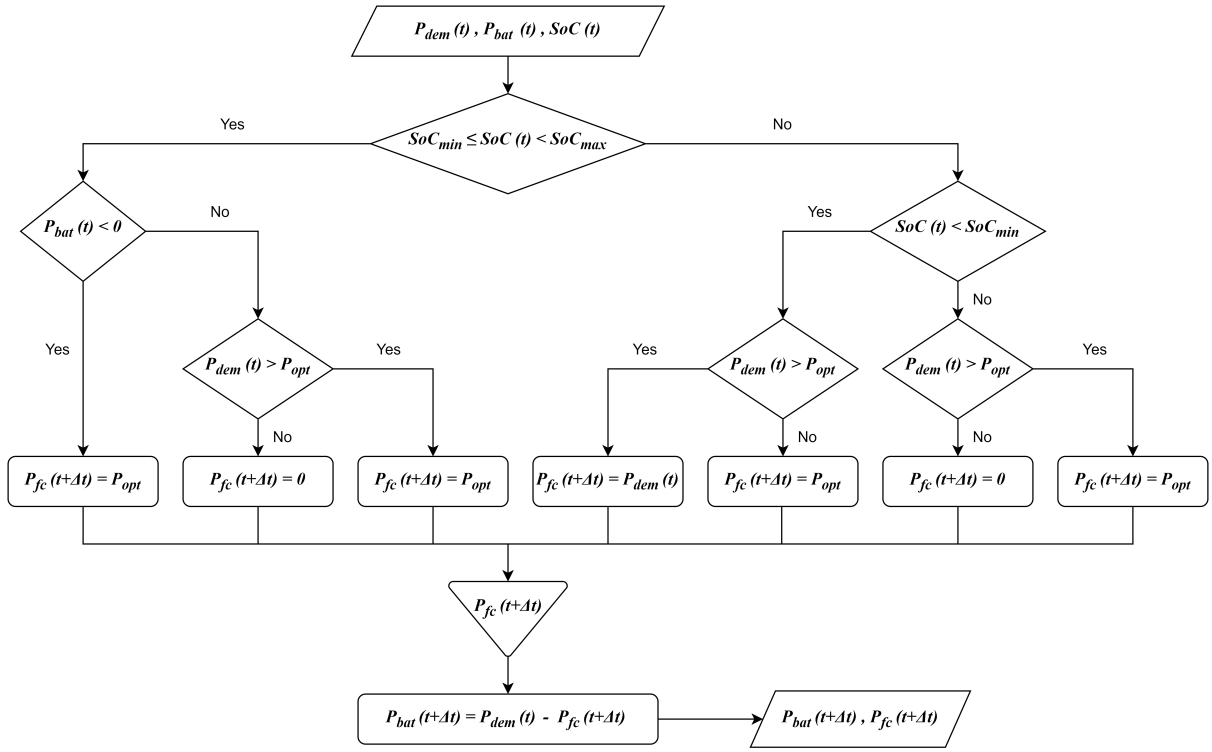

Figure 4.1: Flow chart for the Rule-based control

	$P_{dem}(t) = 0kW$	$0 < P_{dem}(t) \leq P_{opt}$	$P_{dem}(t) > P_{opt}$
$SoC(t) < SoC_{min}$	Fuel-cell: ON Battery: Charging (until SoC reaches SoC_{min}) $P_{fc} = -P_{bat} = P_{opt}$	Fuel-cell: ON Battery: Charging (until SoC reaches SoC_{min}) $P_{fc} = P_{opt}$ $P_{bat} = P_{dem} - P_{fc}$	Fuel-cell: ON Battery: OFF $P_{fc} = P_{dem}$
Battery mode in previous time step: Charging $SoC_{min} \leq SoC(t) < SoC_{max}$	Fuel-cell: ON Battery: Charging (until SoC reaches SoC_{min}) $P_{fc} = -P_{bat} = P_{opt}$	Fuel-cell: ON Battery: Charging (until SoC reaches SoC_{min}) $P_{fc} = P_{opt}$ $P_{bat} = P_{dem} - P_{fc}$	Fuel-cell: ON Battery:Discharging $P_{fc} = P_{opt}$ $P_{bat} = P_{dem} - P_{fc}$
Battery mode in previous time step:Discharging	Fuel-cell: OFF Battery: OFF	Fuel-cell: OFF Battery:Discharging $P_{bat} = P_{dem}$	Fuel-cell: ON Battery: Discharging $P_{fc} = P_{opt}$ $P_{bat} = P_{dem} - P_{fc}$
$SoC(t) \geq SoC_{max}$	Fuel-cell: OFF Battery: OFF	Fuel-cell: OFF Battery:Discharging $P_{bat} = P_{dem}$	Fuel-cell: ON Battery:Discharging $P_{fc} = P_{opt}$ $P_{bat} = P_{dem} - P_{fc}$

Table 4.1: Rule-based control

4.2. Quadratic Programming

Quadratic Programming is a nonlinear optimization problem with a quadratic cost function and linear constraints of the form [39]:

$$\text{Minimize} \quad J = \frac{1}{2} \cdot z^T H z + f^T \cdot z$$

subject to:

$$A_{eq} \cdot z = B_{eq} \tag{4.1}$$

$$A_{ineq} \cdot z \leq B_{ineq} \tag{4.2}$$

$$lb \leq z \leq ub \tag{4.3}$$

The Quadratic Programming (QP) representation allows us to expand the energy management problem into a detailed mathematical formulation. This formulation includes state-space equations, bounded constraints, and specific objective functions. For this particular energy management problem, we define the decision variable z as follows:

$$z^T = \begin{bmatrix} SoC(1) & u_{fc}(1) & SoC(2) & u_{fc}(2) & SoC(3) & u_{fc}(3) & \cdots & SoC(N+1) \end{bmatrix} \tag{4.4}$$

where the subscripts of SoC and u_{fc} are the time steps, and N is the total number of time steps in the drive cycle.

This specific system's optimization control strategy represented is represented in the form of Quadratic Programming problem as follows:

$$\text{Minimize} \quad J = \sum_{i=1}^{N} \left[\omega_1 \cdot u_{fc}(i) + \omega_2 \cdot \left(u_{fc}(i) - \frac{P_{opt}}{k_{fc}} \right)^2 \right]$$

subject to:

$$SoC(i+1) = SoC(i) + \frac{k_{fc} \cdot \tau_s \cdot u_{fc}(i)}{E_{bat}} - \frac{[P_{dem}(i) + P_{loss}(i) + P_d(i)] \cdot \tau_s}{E_{bat}} \tag{4.5}$$

$$y(i+1) = SoC(i+1) \tag{4.6}$$

$$SoC_{min} \leq SoC(i+1) \leq SoC_{max} \tag{4.7}$$

$$0 \leq u_{fc}(i) \leq 1 \tag{4.8}$$

$$-1 \leq \left[\frac{P_{dem}(i) + P_{loss}(i) + P_d(i) - (k_{fc} \cdot u_{fc}(i))}{k_{bat}} \right] \leq 1 \tag{4.9}$$

$$\frac{-\epsilon}{k_{fc}} \leq [u_{fc}(i+1) - u_{fc}(i)] \leq \frac{\epsilon}{k_{fc}} \tag{4.10}$$

$$\forall i \in [1, N]$$

This is a multi-criteria single-objective optimization problem where the cost function has two main goals. The first weighted part of this objective function minimizes the normalized fuel cell power or the control variable over the entire power profile, thereby reducing the total fuel consumption. This is given a weighting factor of ω_1. The second part tries to minimize the error between power produced by the fuel cell at any instant and the optimal fuel cell power P_{opt}. Reducing this error helps the fuel cell to run at its maximum efficiency. The weighting factor ω_2 is determined such that this part of the objective function

is active when u_{fc} > 0, i.e., when the fuel cell is turned on. To keep the priorities of the objectives consistent with each other, all the terms are normalized.

The problem is subject to multiple constraints, which describe the behaviour of the system. The first two constraints, Equation 4.5 and Equation 4.6 are the state-space equations, describing the system dynamics. Equation 4.7 limits the range of the battery state of charge to $[SoC_{min}, SoC_{max}]$. An SoC of 1 (or 100 %) indicates a fully charged battery and 0 indicates a fully discharged one. For normal operation, due to battery health considerations [40], the battery's state of charge is never allowed to go to 0 or 1. This constraint addresses that issue. Equation 4.8 restricts u_{fc} to the range [0,1], and consequently constrains the output power of the fuel cell to stay within its operational range. Similarly, Equation 4.9 limits the power produced by the battery to the range $[-k_{bat}, k_{bat}]$, where k_{bat} is the maximum power that can be produced by the battery. As described in the previous section, negative values of the battery power indicate charging and positive values, discharging.

The final constraint, Equation 4.10, limits the rate of change of the power output of fuel cell. This ensures that significant power variations are handled by the battery and not the fuel cell. The absolute value of change in u_{fc} in the sampling time is limited to ϵ.

4.3. Hierarchical Model Predictive Control

The Hierarchical Model Predictive Control (HMPC) functions similarly to classical MPC by performing real-time optimization over a prediction horizon. As shown in Figure 4.2, the reference values for the battery state of charge is obtained from the upper level. These values are the results of global optimization, which in this case is chosen as a Quadratic Programming problem, computed prior to the operation of the vessel. An ideal power profile, which is created by anticipating and approximating the upcoming drive cycle of the boat, is made available to the global optimizer as an input, and the problem is then optimized over the entire period of operation. These globally optimized reference values for the SoC are subsequently passed to the lower level MPC, where they serve as targets during the real-time operation of the vessel. The reference values give the lower level MPC an idea of what it can expect in the near future and helps in improving its predictive potential. The MPC continually compares the real-time system behavior with these reference values and adjusts the power split between the fuel cell and the battery accordingly.

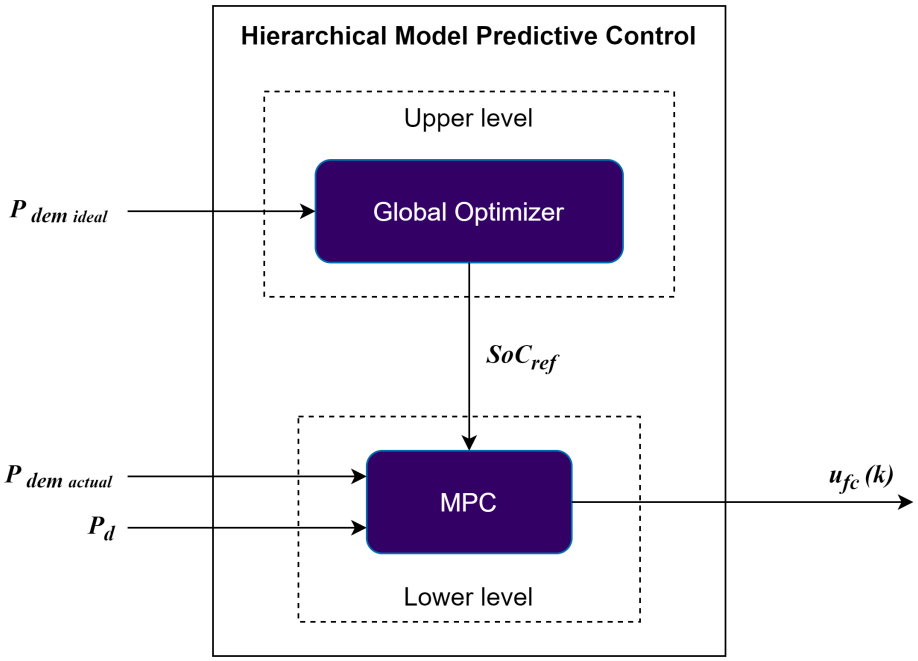

Figure 4.2: Hierarchical MPC

The HMPC optimizes the control problem over a prediction horizon N_p, solves the values for the control and state variables over this horizon, but implements only the first control variable. This process is then repeated over the entire drive cycle. The control problem for every time step is defined as follows:

Minimize

$$J = \sum_{i=0}^{N_p-1} \left[\omega_1 \cdot u_{fc}(k+i) + \omega_2 \cdot \left(u_{fc}(k+i) - \frac{P_{opt}}{k_{fc}} \right)^2 + \omega_3 \cdot (y(k+i+1) - SoC_{ref}(k+i+1))^2 \right]$$

subject to:

$$SoC(k+i+1) = SoC(k+i) + \frac{k_{fc} \cdot u_{fc}(k+i) \cdot \tau_s}{E_{bat}} - \frac{(P_{dem}(k+i) + P_{loss}(k+i) + P_d(k+i)) \cdot \tau_s}{E_{bat}} \tag{4.11}$$

$$y(k+i+1) = SoC(k+i+1) \tag{4.12}$$

$$SoC_{min} \leq SoC(k+i+1) \leq SoC_{max} \tag{4.13}$$

$$0 \leq u_{fc}(k+i) \leq 1 \tag{4.14}$$

$$-1 \leq \left[\frac{P_{dem}(k+i) + P_{loss}(k+i) + P_d(k+i) - (k_{fc} \cdot u_{fc}(k+i))}{k_{bat}} \right] \leq 1 \tag{4.15}$$

$$\frac{-\epsilon}{k_{fc}} \leq [u_{fc}(k+i) - u_{fc}(k+i-1)] \leq \frac{\epsilon}{k_{fc}} \tag{4.16}$$

$$\forall i \in [0, N_p - 1]$$

The objective function of the HMPC focuses on three key aspects: minimizing fuel consumption, ensuring the fuel cell operates at its optimal power, and reducing the error between the actual battery SoC and the reference SoC value obtained from the Quadratic Programming problem in the upper level. These are prioritized by using the weights ω_1, ω_2 and ω_3 respectively. $\omega_1 \cdot u_{fc}(k+i)$ minimizes the fuel cell's power output over the predictive horizon, thereby reducing the generated power, and consequently, hydrogen consumption. The term $\omega_2 \cdot \left(u_{fc}(k+i) - \frac{P_{opt}}{k_{fc}} \right)^2$ minimizes the squared error between the fuel cell's output and its optimal power, pushing the system to operate at maximum efficiency. Finally, $\omega_3 \cdot (y(k+i+1) - SoC_{ref}(k+i+1))^2$ minimizes the error between the actual SoC and the reference SoC over the horizon to keep the system aligned with the global optimizer's solution and follow its trend. k is the time-step during the optimization and i denotes the horizon steps.

The upper level global optimization does not consider the disturbances (winds or waves) or changes in physical characteristics of the system (such as additional cargo or people onboard the vessel) which are not known beforehand. However, the lower level of the HMPC, working in real-time, adjusts for these disturbances faced by the system, while still meeting the actual power demands. Even though the reference values represent the ideal conditions, and not the actual operational profile, the control strategy gets a general idea of what it can expect in the future. This helps it choose when to switch on the fuel cell and when to turn it off with minimal variations in its power production.

5

Results

In this chapter, the parameters for the optimization strategies are defined in section 5.1. The three control strategies are then verified using tests to ensure they obey all the constraints, in section 5.2. Robustness checks are done on the Hierarchical MPC in section 5.3. Finally, in section 5.4, the Rule-based control, Hierarchical MPC and QP are compared based on the KPI to answer the research questions.

To run the simulations for testing, the values of disturbances in power demand, P_d, were considered as a random variable with a specified range and an upper and lower limit for $\frac{dP_d}{dt}$. In testing, the range for P_d was set as $[-0.1P_{dem_{max}}, 0.1P_{dem_{max}}]$. For comparing the controls however, the range was set as $[-0.2P_{dem_{max}}, 0.2P_{dem_{max}}]$, to get a more realistic power variation. The power profile was created based on the data retrieved from the H2C boat. The characteristics of the power demand and disturbance used in different drive cycles are described in the Table 5.2.

5.1. Parameter Tuning for QP and HMPC

The weights used in the objective function of the optimization strategies are crucial for shaping the desired behavior of the control strategies. Multiple considerations in the optimal control problem had to be combined into a single objective function, but these criteria were not diametrically opposed—improving one did not necessarily worsen the others in terms of optimality. So, to ensure optimal performance, a Grid search method was employed to fine-tune the weights of the various criteria in the objective function. Using the Grid search, the weights (ω) assumed by the multiple criteria in the objective function were selected by dividing the range [0,1] into equally spaced partitions. This allowed for systematic testing of different values to find the most optimal ω values. For the Quadratic Programming (QP) strategy, the optimal values for ω_1 and ω_2 were determined in this way. In the Hierarchical MPC, for simplicity and to maintain consistency between its upper and lower level, the ratio between ω_1 and ω_2 from the QP was preserved, while the optimal value for ω_3 was tuned with respect to the sum of the first two weights.

Another parameter that had to be chosen carefully was the prediction horizon N_p for the HMPC. A balance had to be struck between ensuring that the fuel consumption converged to an optimal value over the drive cycle while keeping the computational complexity manageable. This trade-off helped determine the best value for N_p, ensuring efficient yet practical control performance.

Objective function weights

For the QP problem, the weights ω_1 and ω_2 were defined such that their sum always equaled to 1. In this Grid search approach, the weights were systematically varied from 0 to 1, the optimization problem was solved for each set of values, and the corresponding normalized objective function was calculated. Normalizing the terms within the objective function helped ensure that each term received an appropriate weight, minimizing any bias. Since this was a multi-criteria single objective minimization

problem, the weight combination that yielded the lowest value of the objective function was selected as optimal.

As shown in Figure 5.1, ω_1 was plotted on the x-axis and the solution for the objective function on the y-axis, the minimum solution occured at an ω_1 value of 0.78. This implied that ω_2 has a value of 0.22 at this point. Thus, for the Quadratic Programming problem, the optimal values for ω_1 and ω_2 were 0.78 and 0.22 respectively.

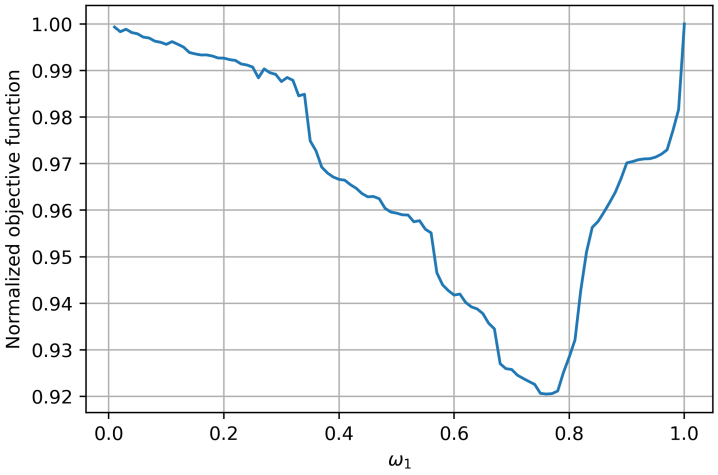

Figure 5.1: Grid search for ω determination in QP

In HMPC, since the optimization problem was similar to QP, and to make the test simple, the ratio of ω_1 to ω_2 was kept the same as before. The weight for reference tracking, ω_3 was varied with respect to the sum of ω_1 and ω_2, getting to the relation:

$$\omega_3 = 1 - (\omega_1 + \omega_2)$$

while maintaining the ratio,

$$\frac{\omega_1}{\omega_1 + \omega_2} = 0.78$$

The value of ω_3 was varied in a similar fashion as before, and the normalized objective function of the HMPC problem was evaluated over the entire drive cycle. As with the grid search process for QP method, the goal was to find the values of the weights corresponding to the lowest value of the objective function.

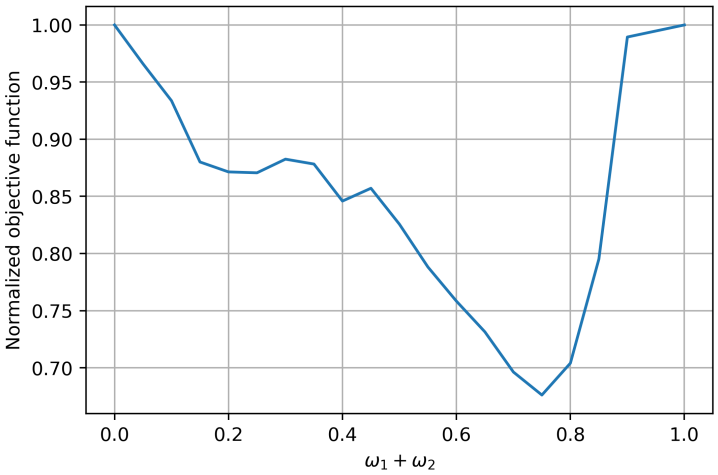

Figure 5.2: Grid search for ω determination in HMPC

Thus, from Figure 5.2, the value for ω_3 was selected as 0.25. The values of ω_1 and ω_2 were calculated as 0.585 and 0.165 respectively.

Prediction Horizon

Identifying the prediction horizon, N_p for the HMPC involved balancing fuel consumption and computational complexity. As N_p increased, the computational time and complexity of the HMPC optimization problem increased. To find the optimal horizon, the HMPC was run multiple times for the same power profile using different values of N_p, and the total fuel consumption was plotted against N_p (as shown in Figure 5.3).

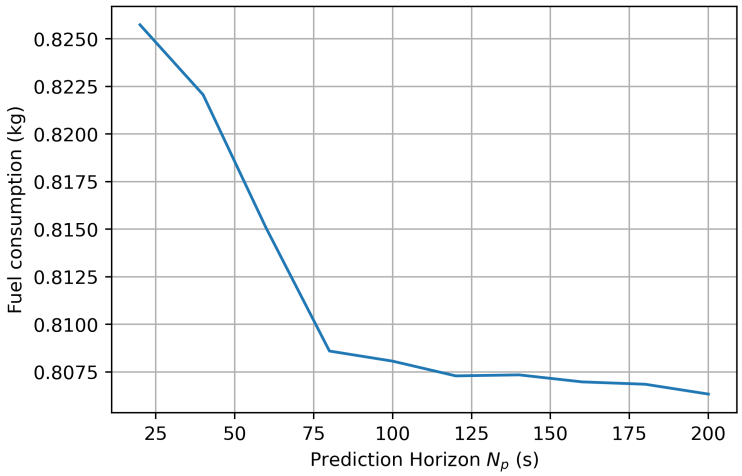

Figure 5.3: Test for N_p determination

From Figure 5.3, it was clear that increase in N_p led to better optimization results. However, after a certain point, which in this case was an N_p of 80 seconds, the fuel consumption started to converge, which meant that further increase in the prediction horizon did not result in significant reductions in fuel consumption. Therefore, a value of 80 seconds was taken as the optimal value of N_p.

5.2. Constraint Feasibility Check

Feasibility of the three control strategies were tested through a series of tests designed to ensure that they behaved as expected. These tests focused on confirming that key operational constraints were met across different scenarios. The tests were designed to ensure that the model consistently adhered to the following rules:

- Test 1: SoC must remain within the prescribed range of $[SoC_{min}, SoC_{max}]$
- Test 2: Rate of change of the fuel cell's power output should be within the range $[-\epsilon, \epsilon]$
- Test 3: The power produced by both the fuel cell and the battery must not exceed their respective limits.

Different power profiles were employed during the tests. These profiles were not always identical to the one depicted in Figure 3.3a. Some were specifically crafted to check whether the controls effectively managed the plant's parameters, keeping them within their prescribed limits.

Test 1

This test evaluated whether the battery's state of charge (SoC) remained within the defined limits under various conditions. To assess this, the values of SoC_{min} and SoC_{max} were varied to ensure that the SoC consistently stayed within the allowable bounds, regardless of the plant's conditions or the power demand. This flexibility in defining safe operating limits for the battery was tested for all three strategies.

The results of this test are shown in Figure 5.4. The maximum and minimum allowable values of battery SoC are shown by the red and green dotted lines respectively.

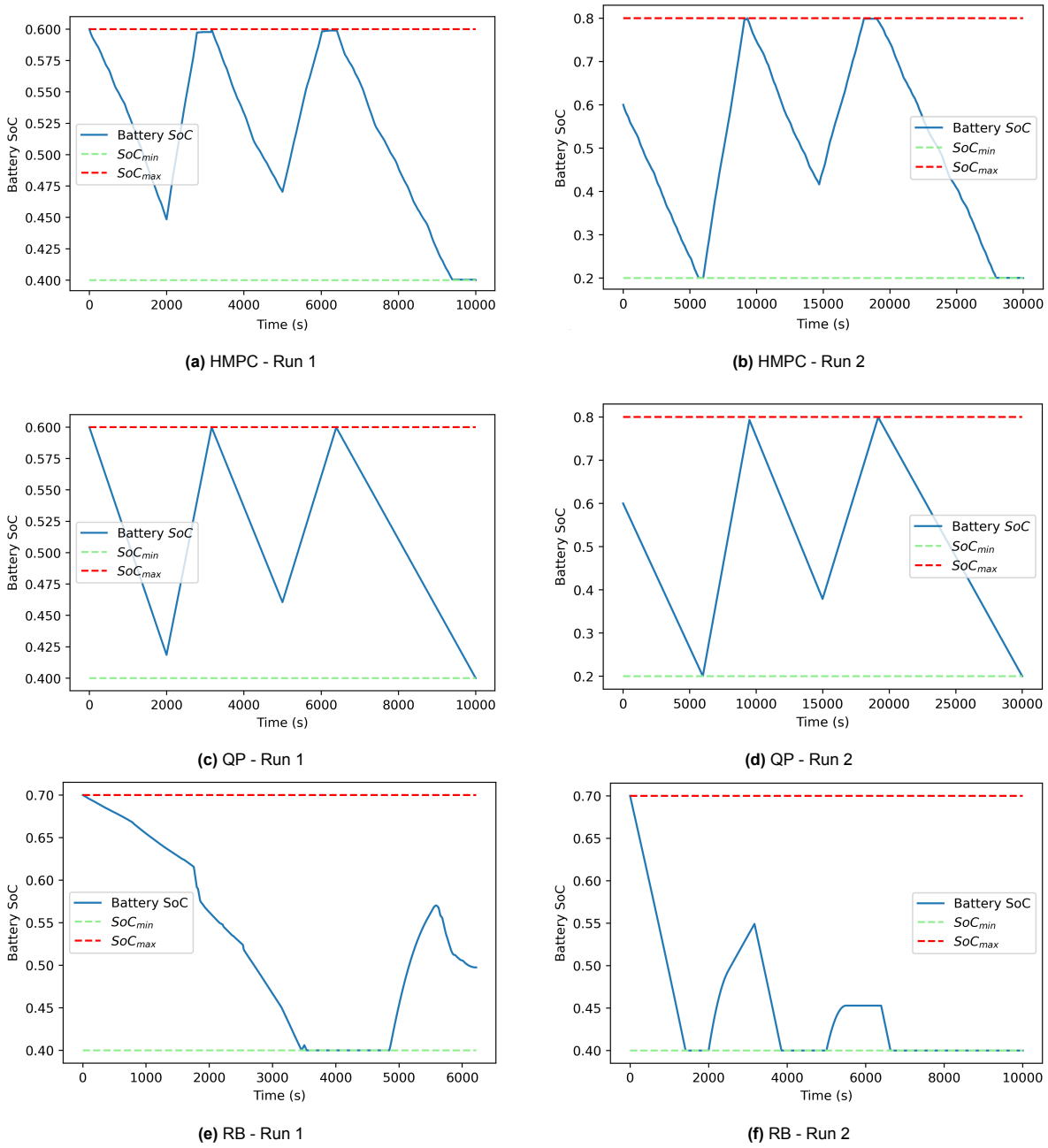

(a) HMPC - Run 1

(b) HMPC - Run 2

(c) QP - Run 1

(d) QP - Run 2

(e) RB - Run 1

(f) RB - Run 2

Figure 5.4: Verification Test 1

The plots confirm that the system's behavior adheres to the constraints, as the SoC values are maintained within the specified range across all scenarios, whether the battery is charging, discharging, or turned off.

Test 2

This test evaluated whether the rate of change in the power delivered by the fuel cell adhered to the specified limit, as outlined in the beginning of chapter 4. The absolute rate of change of fuel cell power, $\left(\frac{dP_{fc}}{dt}\right)$, was constrained to be less than or equal to ϵ. A mathematical constraint for the range was used

in the optimization problem for the two optimization-based controls, while a rate limiter was applied for the rule-based control.

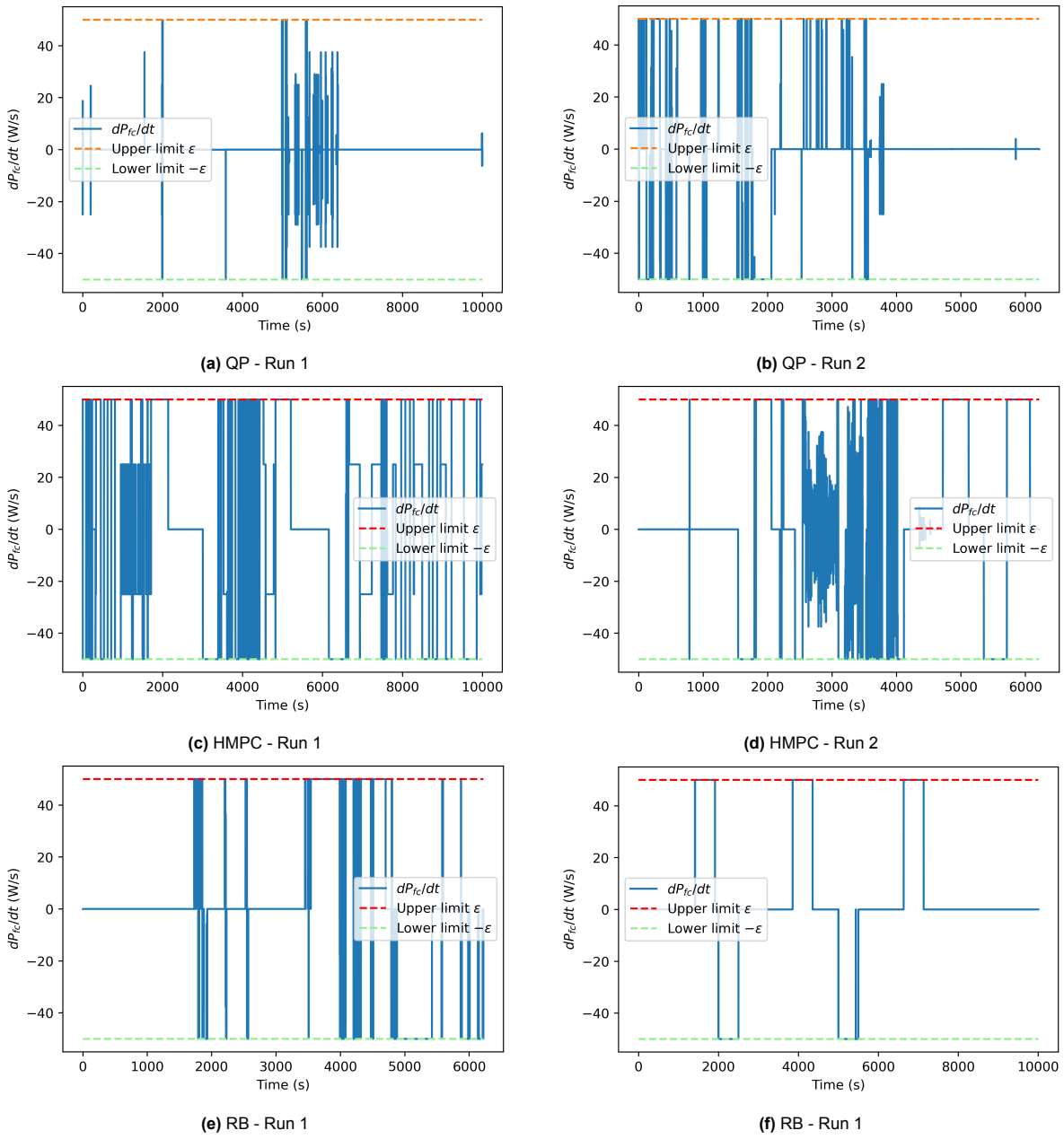

(a) QP - Run 1

(b) QP - Run 2

(c) HMPC - Run 1

(d) HMPC - Run 2

(e) RB - Run 1

(f) RB - Run 1

Figure 5.5: Verification Test 2

As shown in the Figure 5.5, all the control strategies satisfied this operational limitation of the fuel cell. This ensured that, once the real value of ϵ is known for a particular fuel cell, the control system would manage the power output without exceeding the specified rate of change. The battery compensated for any necessary adjustments, maintaining power balance while adhering to the fuel cell's operational limits.

Test 3

This test ensured that the power requested from both the fuel cell and battery adhered to their operational capacity. The maximum power capacity of the fuel cell and battery were defined by k_{fc} and k_{bat} respectively. For the fuel cell, the minimum power is 0 kW, while the battery could handle nega-

tive values during charging, with a minimum of $-k_{bat}$. Therefore, the power requested by the control strategies must align with these capacity limits.

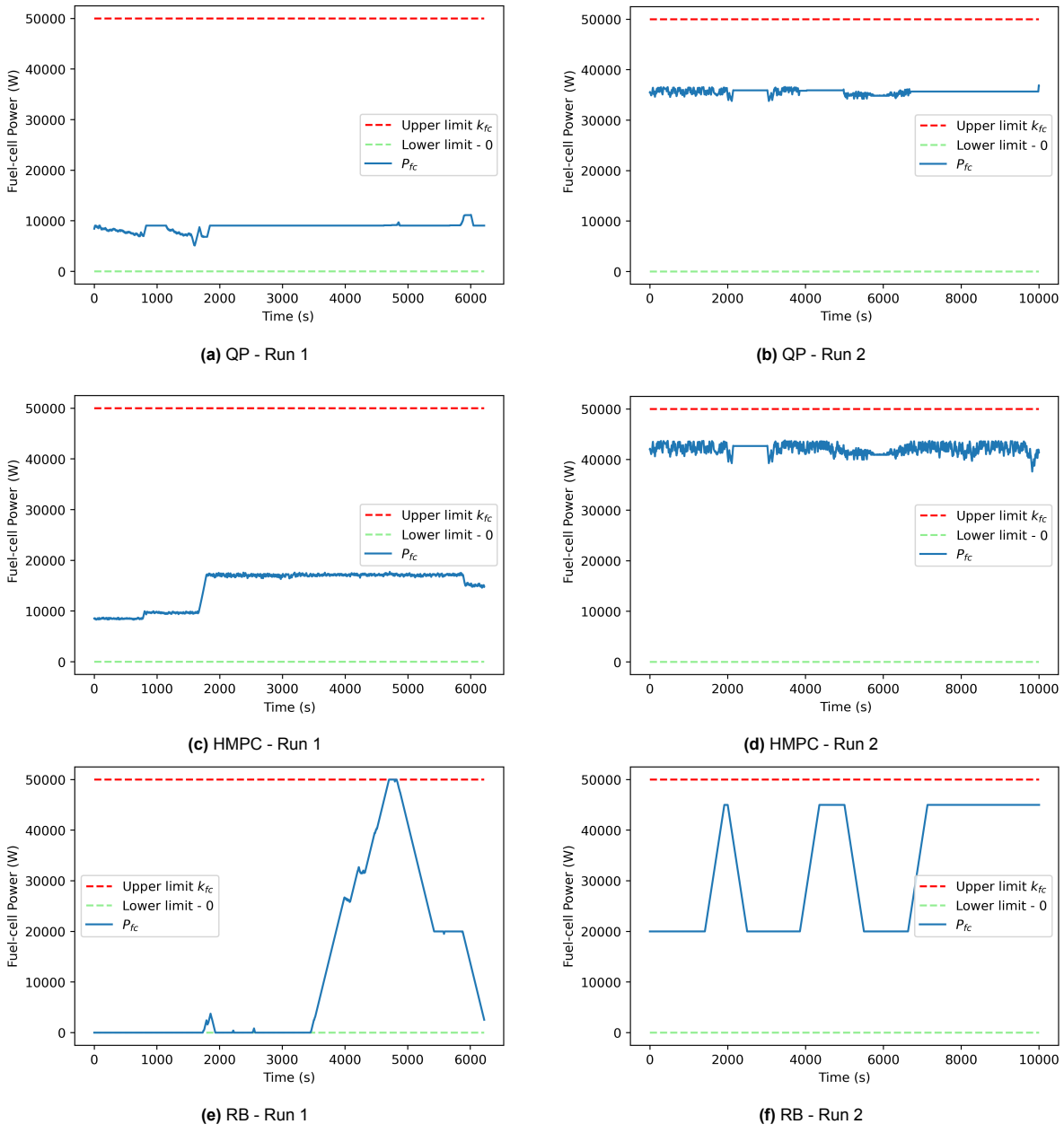

(a) QP - Run 1

(b) QP - Run 2

(c) HMPC - Run 1

(d) HMPC - Run 2

(e) RB - Run 1

(f) RB - Run 2

Figure 5.6: Verification Test 3 - P_{fc}

In this test, the working range of the fuel cell was kept between 0 and 50 kW. As illustrated in Figure 5.6, for the QP and HMPC, P_{fc} did not assume the extreme values unless absolutely necessary, because the objective function aimed to minimize the fuel cell power. When the fuel cell operated, P_{fc} was pulled to the value P_{opt}. However, for RB control, due to the lack of predictive capabilities or foresight, the fuel cell had to take over and satisfy the demands when the battery charge was depleted. Despite this, the test proved that the operable range of the fuel cell power is respected by it, as demonstrated in Figure 5.6e.

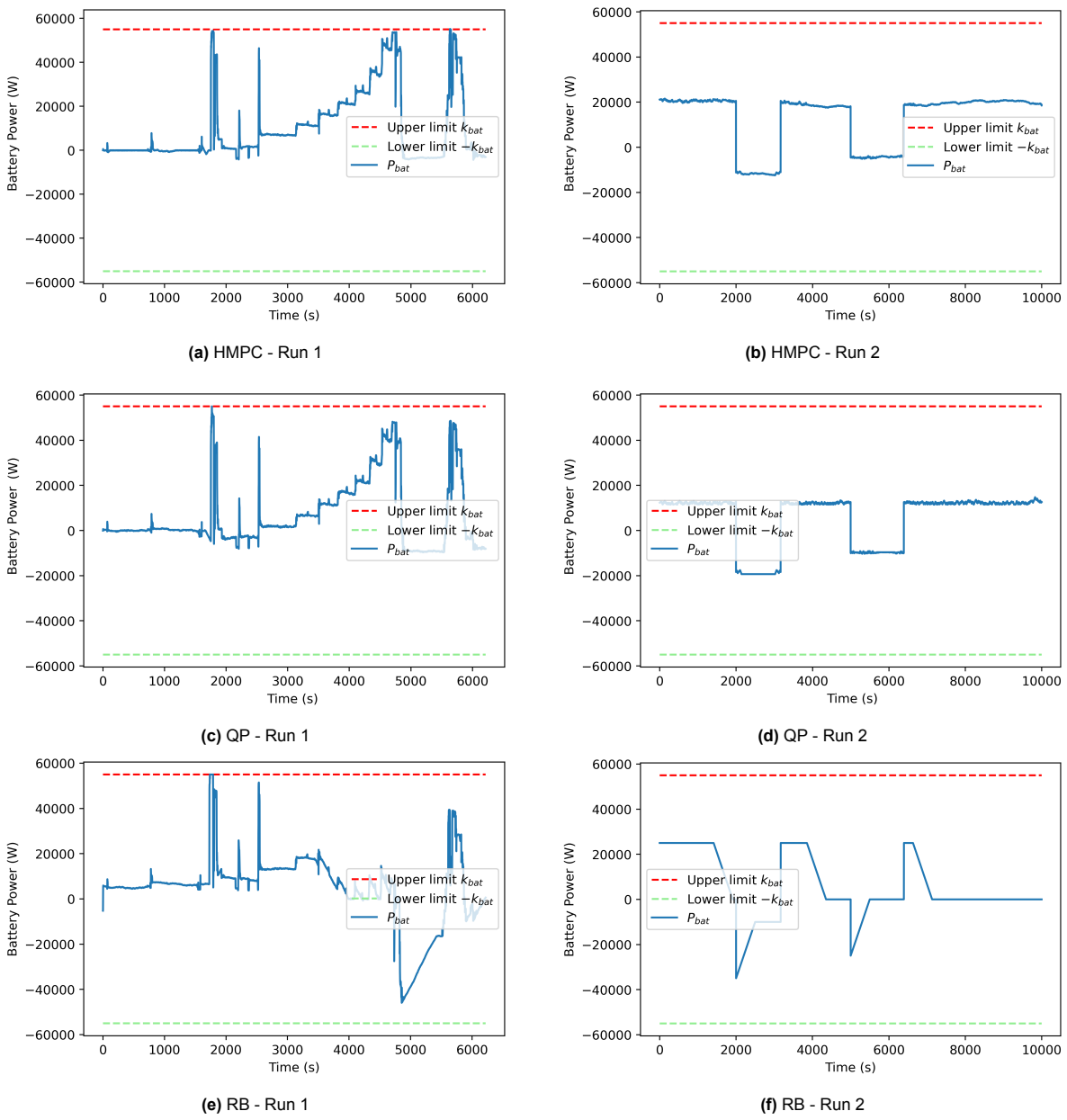

(a) HMPC - Run 1

(b) HMPC - Run 2

(c) QP - Run 1

(d) QP - Run 2

(e) RB - Run 1

(f) RB - Run 2

Figure 5.7: Verification Test 3 - P_{bat}

Since the battery's power output is used to balance the power demand while the fuel cell's power output is more regulated, the power requested from or delivered to the battery, P_{bat}, varied more significantly compared to the fuel cell power, P_{fc}. Regardless of whether the battery is charging or discharging, all three controls ensured that the power levels remained within the specified limits of the battery.

These tests confirmed that the control strategies adhered to the fundamental properties and requirements of the system. The constraints on the parameters functioned as intended, thus verifying the proper operation of the controls and their alignment with the modelled specifications.

5.3. Robustness Check

The entire system can be illustrated using a control diagram as shown in Figure 5.8. The closed-loop system consists of the controller and the plant, with the plant modelled using state-space equations.

The controller's transfer function is denoted by K, and the plant's transfer function is represented by P. The reference signal is labelled r, the output signal is y, the control signal is u, and the error signal is e. P_{dem} refers to the power demand (an exogenous input), and P_d represents the disturbances in the requested power. It is assumed that there is an absence of any noise inputs.

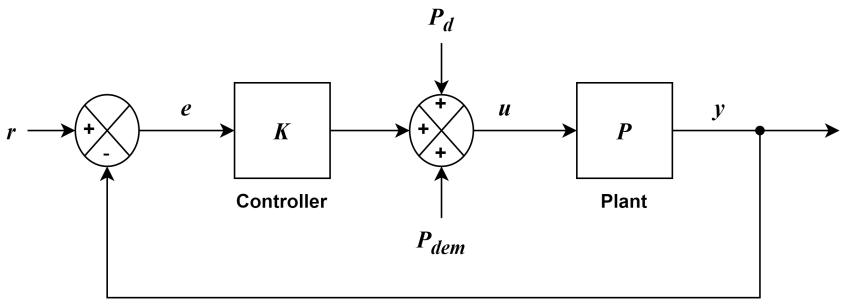

Figure 5.8: Control Diagram

Robustness refers to a system's ability to withstand or handle adverse conditions effectively, particularly in a closed-loop configuration where it must remain stable and perform well despite uncertainties or variations in the plant or controller behavior. During the modelling phase, approximations, disturbances, noise, and other unknown factors can cause the model's dynamics to deviate from the actual system dynamics. To ensure that the system remains effective under these conditions, robustness tests are performed.

The robustness of this system was evaluated through the use of sensitivity functions, which quantify the system's response to disturbances and noise. The sensitivity and complementary sensitivity functions were defined for all signal inputs, and Bode plots were used to analyze these functions. This analysis provided insight into the system's ability to maintain performance despite uncertainties.

$$\dot{x}(t) = A_c x(t) + B_c u(t) + E_c d(t) \tag{5.1}$$

$$y(t) = C_c x(t) + D_c u(t) + F_c d(t)$$

$$u(t) = \begin{bmatrix} u_{fc}(t) \\ P_{dem}(t) \end{bmatrix}, d(t) = \begin{bmatrix} P_{loss}(t) \\ P_d(t) \end{bmatrix},$$

$$A_c = 0, \quad B_c = \begin{bmatrix} \frac{k_{fc}}{E_{bat}} & \frac{-1}{E_{bat}} \end{bmatrix}, \quad E_c = \begin{bmatrix} \frac{-1}{E_{bat}} & \frac{-1}{E_{bat}} \end{bmatrix}, , \quad C_c = 1 \quad D = \begin{bmatrix} 0 & 0 \end{bmatrix}, \quad F_c = \begin{bmatrix} 0 & 0 \end{bmatrix}$$

The first step involved determining the transfer functions for all system inputs. These transfer functions were then used to compute the loop transfer functions, which were subsequently utilized to derive the sensitivity and complementary sensitivity functions. For this test, the plant had to be defined as a continuous state-space equation instead of the discrete model created for QP and MPC. The continuous model was therefore rewritten in the continuous time domain as Equation 5.1. Based on this state-space model, the basic transfer functions for u_{fc}, P_{dem} and P_d, respectively, were calculated as follows:

$$G_u(s) = C_c \left(sI - A_c\right)^{-1} B_{c1} + D_{c1} \tag{5.2}$$

$$G_p(s) = C_c \left(sI - A_c\right)^{-1} B_{c2} + D_{c2} \tag{5.3}$$

$$G_d(s) = C_c \left(sI - A_c\right)^{-1} E_c + F_c \tag{5.4}$$

where B_{c1} and B_{c2} were the first and second elements of the matrix B_c, while D_{c1} and D_{c2} represented the corresponding elements of the matrix D_c from the state-space equation.

The loop transfer functions for each input were then calculated as the product of G, the transfer function corresponding to the respective input, and K, the controller transfer function.

$$L(s) = G(s) \cdot K(s) \tag{5.5}$$

The sensitivity $S(s)$ and the complementary sensitivity functions $T(s)$ were defined from $L(s)$ as follows:

$$S(s) = \frac{1}{1 + L(s)} \tag{5.6}$$

$$T(s) = 1 - S(s) = \frac{L(s)}{1 + L(s)} \tag{5.7}$$

The values of $G(s)$, $L(s)$, $S(s)$ and $T(s)$ for each of the inputs are given in Table 5.1.

Input	$\boldsymbol{G(s)}$	$\boldsymbol{L(s)}$	$\boldsymbol{S(s)}$	$\boldsymbol{T(s)}$
u_{fc}	$\frac{0.0003655}{s}$	$\frac{0.0003655K(s)}{s}$	$\frac{s}{s+0.0003655K(s)}$	$\frac{0.0003655K(s)}{s+0.0003655K(s)}$
P_{dem}	$\frac{-0.00000000731}{s}$	$\frac{-0.00000000731K(s)}{s}$	$\frac{s}{s-0.00000000731K(s)}$	$\frac{-0.00000000731K(s)}{s-0.00000000731K(s)}$
P_d	$\frac{-0.00000000731}{s}$	$\frac{-0.00000000731K(s)}{s}$	$\frac{s}{s-0.00000000731K(s)}$	$\frac{-0.00000000731K(s)}{s-0.00000000731K(s)}$

Table 5.1: Values of transfer functions

Two tests were conducted using the Bode plots of $S(s)$ and $T(s)$ to evaluate the system's robustness. For robustness tests, the controller was assumed to be a simple proportional controller, reducing the transfer function $K(s)$ to a constant. According to Bemporad et al. [41], robustness analysis of Model Predictive Control (MPC) is inherently more complex than its synthesis. While MPC can be designed to robustly stabilize a system, the complexity of analyzing its robustness remains a challenge. MPC naturally stabilizes the closed-loop system, but there are no general methods available to assess its robustness. However, with careful research, a robust MPC can be selected for specific applications. Thus, by using a proportional controller in place of the HMPC, robustness check of the plant was simplified.

Test 1
In the first test, the proportional controller gain, $K(s)$, was varied, and the behaviour of the system was observed through the Bode plot. The plant parameters were kept constant. This helped in assessing the robustness of the system to changes in the controller. The chosen values for proportional controller gain were 0.01, 0.05, 0.1, 0.5, 1, 5, 10, 50 and 100.

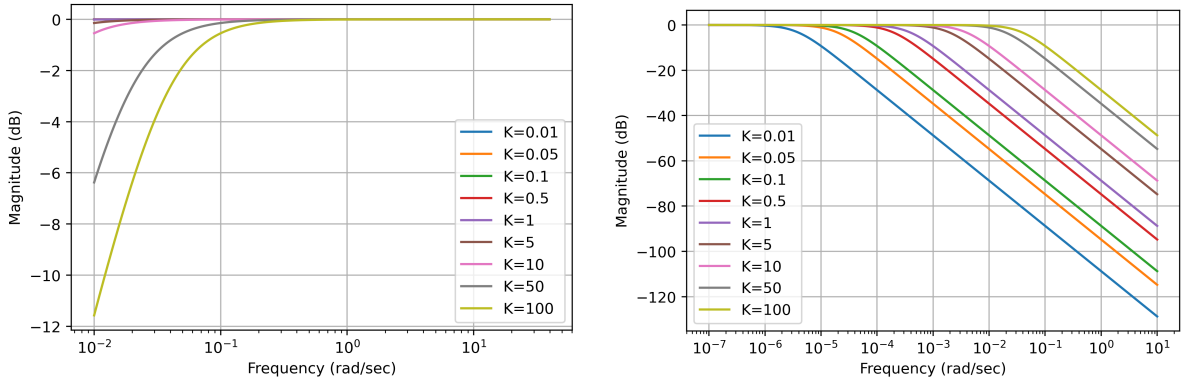

(a) Bode plot of $S(s)$

(b) Bode plot of $T(s)$

Figure 5.9: Test 1 for u_{fc}

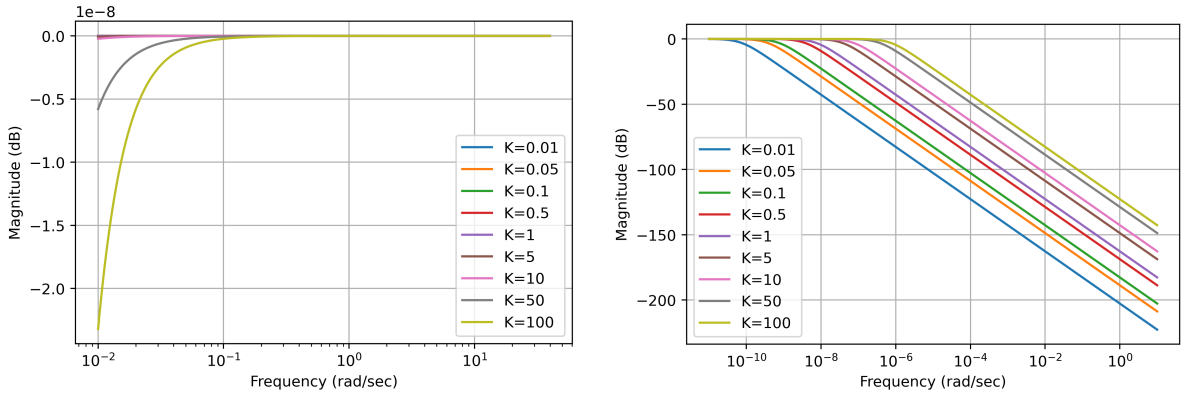

(a) Bode plot of $S(s)$ **(b)** Bode plot of $T(s)$

Figure 5.10: Test 1 for P_{dem}

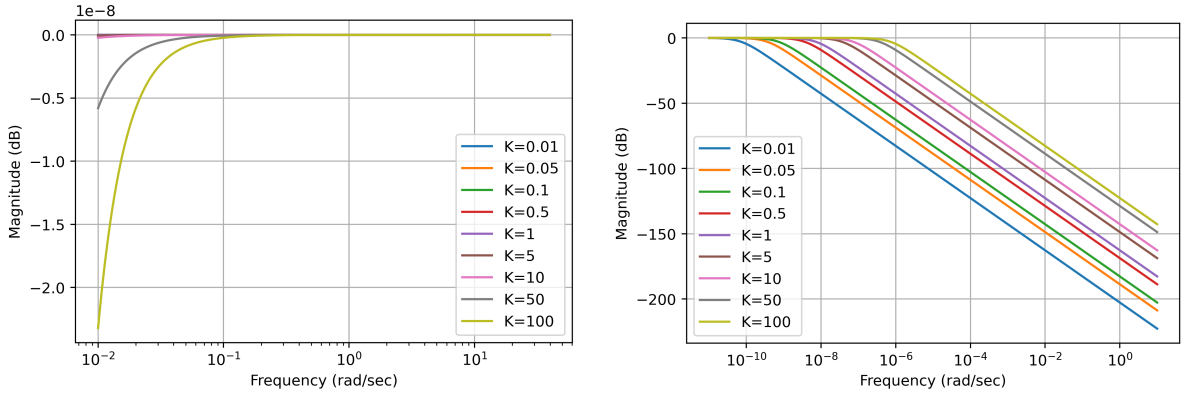

(a) Bode plot of $S(s)$ **(b)** Bode plot of $T(s)$

Figure 5.11: Test 1 for P_d

Test 2

In the second test, $K(s)$ was kept a constant while varying parameters in the plant, specifically B_{c1}, B_{c2} and E_c. The Bode plots were then analyzed. This was used to examine how the system behaved to uncertainties and variations in plant dynamics.

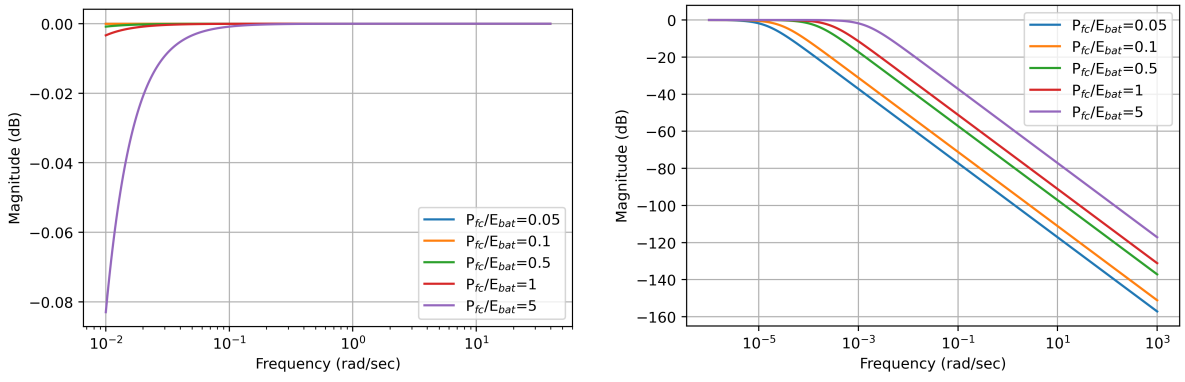

(a) Bode plot of $S(s)$ **(b)** Bode plot of $T(s)$

Figure 5.12: Test 2 for u_{fc}

The parameter varied for the transfer functions of u_{fc} was $\frac{P_{fc}}{E_{bat}}$, with $\frac{P_{fc}}{E_{bat}}$ taking the values of 0.05 s^{-1}, 0.1 s^{-1}, 0.5 s^{-1}, 1 s^{-1} and 5 s^{-1}. For the inputs P_{dem} and P_d, E_{bat} was varied. The values assumed by E_{bat} were 60 kWh, 30 kWh, 10 kWh, 5 kWh and 2.5 kWh.

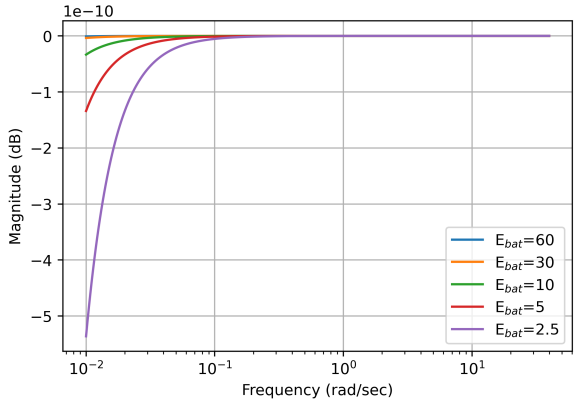

(a) Bode plot of $S(s)$

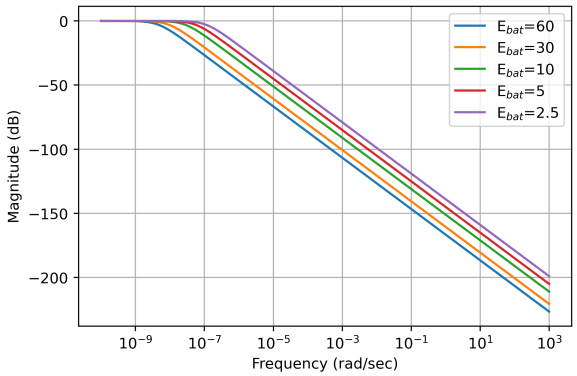

(b) Bode plot of $T(s)$

Figure 5.13: Test 2 for P_{dem}

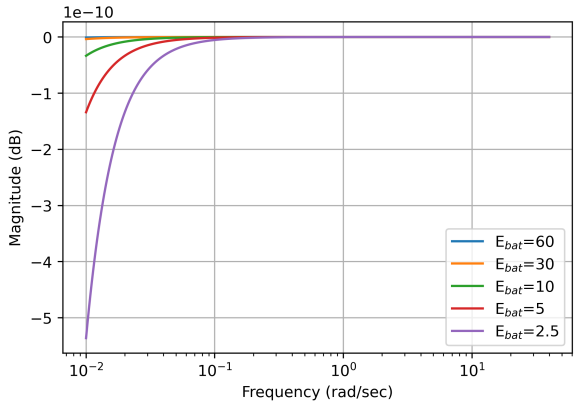

(a) Bode plot of $S(s)$

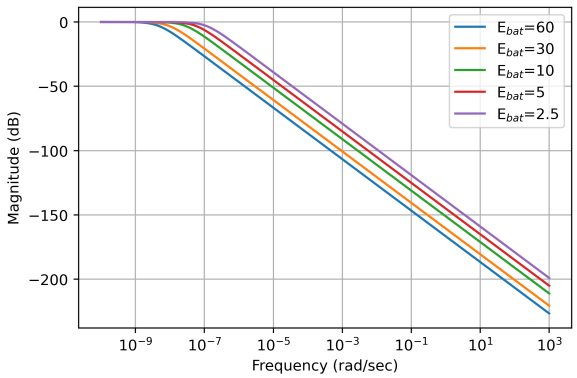

(b) Bode plot of $T(s)$

Figure 5.14: Test 2 for P_d

The Bode plots revealed no peaks, only monotonic changes, and the maximum magnitudes observed were very small. These observations indicated that the system was stable with a high gain margin. The gain margin, a crucial indicator of system stability, confirmed that the system could tolerate significant variations in controller gain and plant dynamics without losing stability. The system effectively accommodated uncertainties without compromising robustness and performance. Furthermore, the absence of peaks suggested strong noise and disturbance rejection. Overall, the test results confirmed that the system exhibited robust performance.

5.4. Control Strategy Comparison

Multiple profiles were run for comparing the control strategies with varying levels of prior knowledge, as shown in Table 5.2. For the first four scenarios, the power profile from the actual boat (Figure 3.3a) was used as the ideal demand power. To simulate real-world conditions, disturbances or variations in power demand were introduced to this profile to obtain the actual power demand. This added disturbance was a stochastic variable with varying ranges of power, with the condition that the actual power demand as such does not take a negative value. In the first four power profiles, the only difference was thus the variation in P_d, quantified as a random variable with an allowable range of $[-0.2P_{dem_{max}}, 0.2P_{dem_{max}}]$.

In the fifth case, the power profile was the same as the fourth, but the reference values obtained from the upper level of HMPC (SoC reference values) were kept constant at 0.65. In the sixth case, the actual power profile was set the same as the ideal profile (i.e., $P_d = 0$).

The plots of results obtained from all three controls in test case II is shown in the figures in this section. Powers produced by the fuel cell and battery, the variation of battery SoC during the operation, and the energy produced by the fuel cell and battery together with the energy demand are plotted for Quadratic Programming, Hierarchical MPC and the Rule-based control.

As shown in Figure 5.15 and Figure 5.16, QP clearly gave a better result in comparison to HMPC. Specifically, with HMPC, the fuel cell power exhibited greater variability and higher levels, leading to increased fluctuations in battery power. The HMPC tried to follow the trend of the reference profile given by the upper level optimizer (solved for the ideal profile). Hence, the fuel consumption was clearly more for HMPC, but it did try to keep close to the globally optimized result. Additionally, both optimization based controls tried to keep P_{fc} close to P_{opt} for majority of the time they worked.

In comparison to the optimization-based controls, the rule-based control is far from perfect. Without any foresight of the upcoming power demand, the fuel cell power management was a struggle after the battery charge was drained. The power produced by the fuel cell and consequently, the energy produced by the fuel cell was higher for the rule-based control. Moreover, it could not always keep P_{fc} close to P_{opt}.

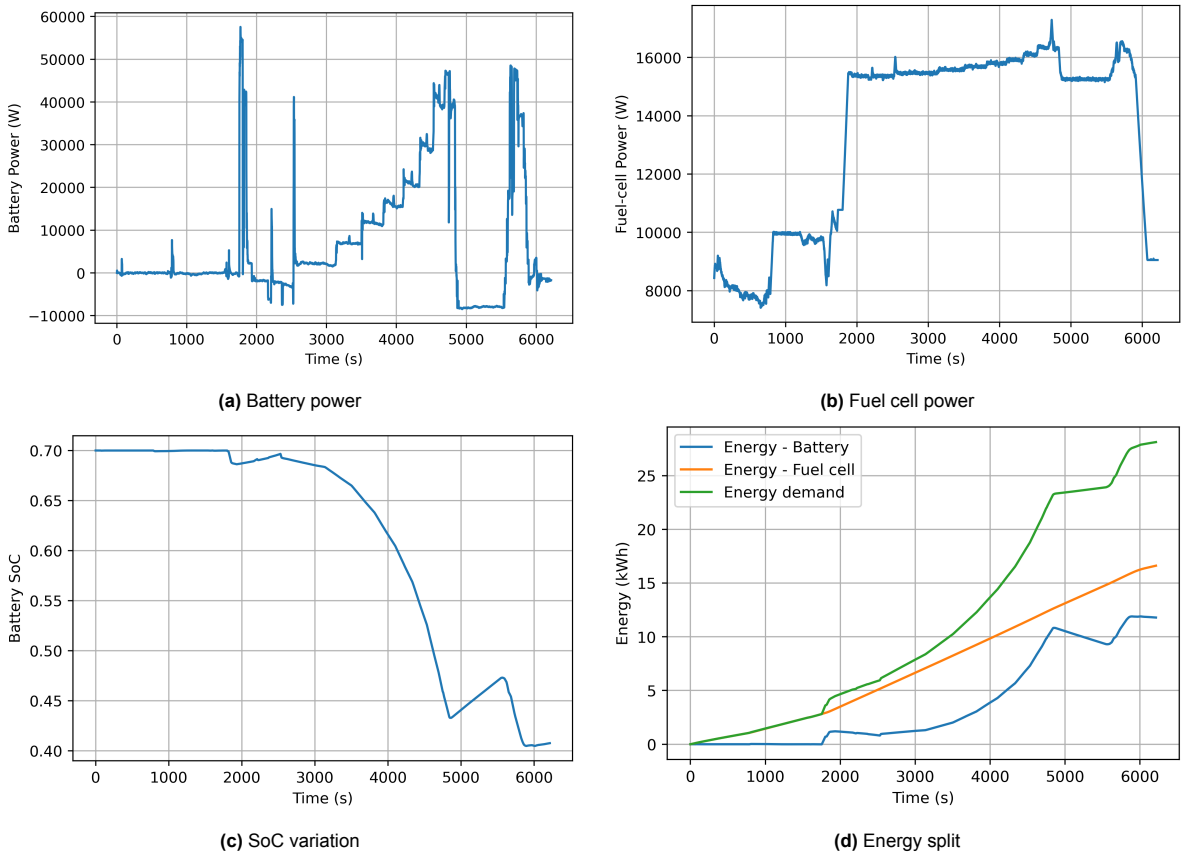

(a) Battery power

(b) Fuel cell power

(c) SoC variation

(d) Energy split

Figure 5.15: Quadratic Programming

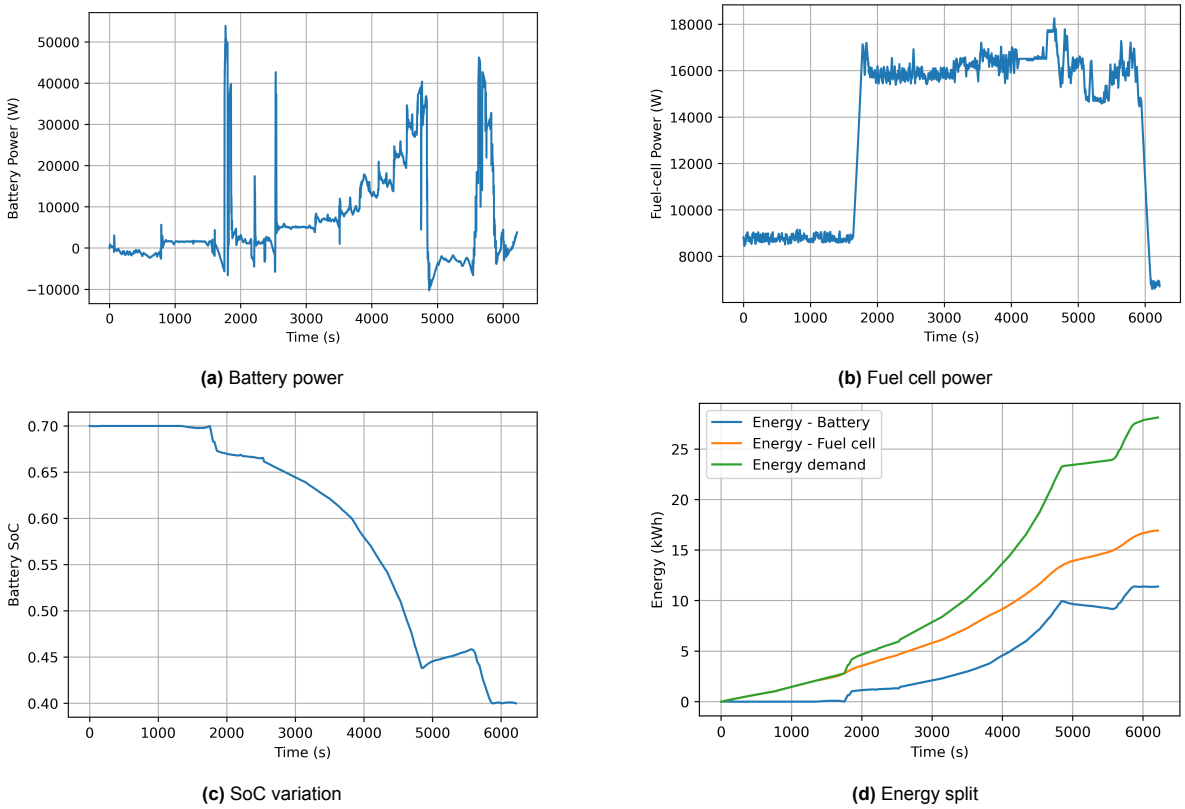

(a) Battery power

(b) Fuel cell power

(c) SoC variation

(d) Energy split

Figure 5.16: Hierarchical MPC

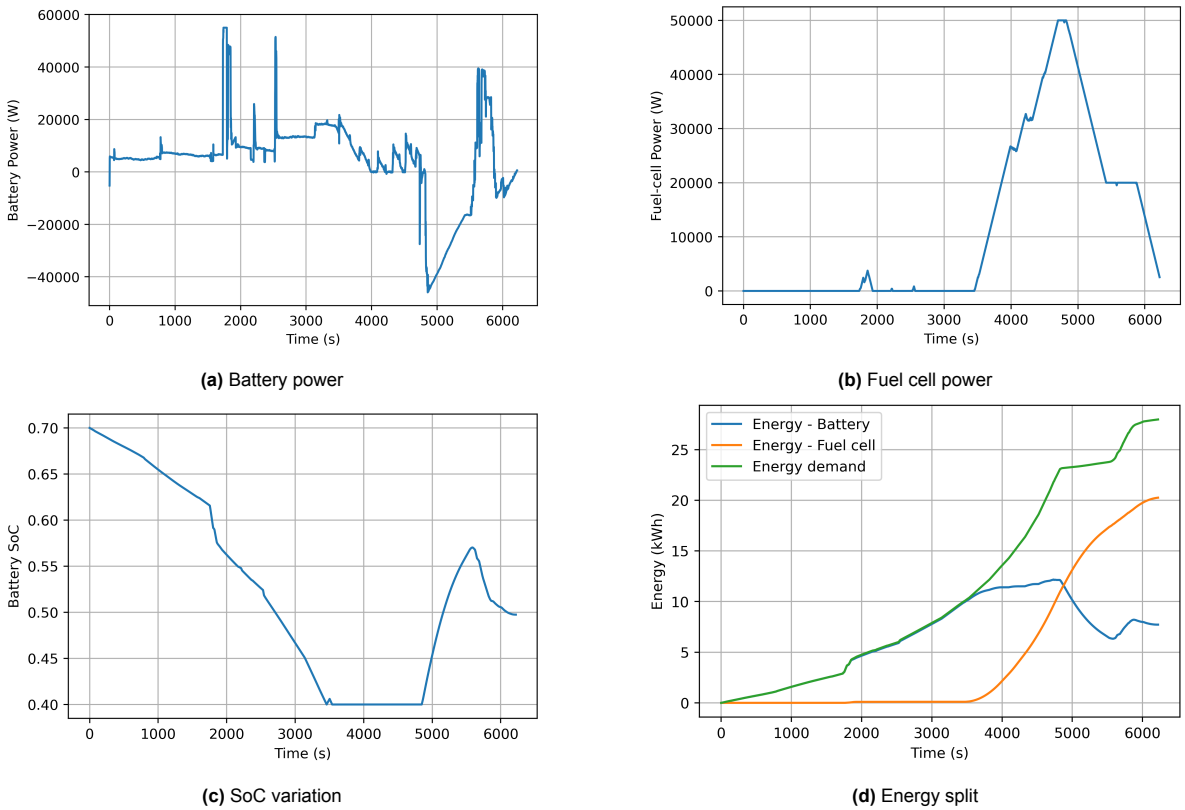

(a) Battery power

(b) Fuel cell power

(c) SoC variation

(d) Energy split

Figure 5.17: Rule-based control

Test case	Fuel consumption (kg)			Characteristics
	RB control	HMPC	QP	
I	1.1143	0.8067	0.7628	$P_d \in [-0.2P_{dem_{max}}, 0.2P_{dem_{max}}]$
II	0.9912	0.8232	0.7344	$P_d \in [-0.2P_{dem_{max}}, 0.2P_{dem_{max}}]$
III	1.0510	0.8197	0.7476	$P_d \in [-0.2P_{dem_{max}}, 0.2P_{dem_{max}}]$
IV	1.1202	0.8303	0.7660	$P_d \in [-0.2P_{dem_{max}}, 0.2P_{dem_{max}}]$
V	1.1202	0.9156	0.7660	P_{dem} same as Test case IV, $SoC_{ref} = 0.65$
VI	0.9794	0.7002	0.6915	$P_{dem_{actual}} = P_{dem_{ideal}}$, $P_d = 0$

Table 5.2: Control strategy comparison

From comparing the control strategies, it could be seen that QP, the offline control strategy, performed the best, providing a globally optimized solution to the control problem. The Hierarchical MPC had results closer to that of QP in the first four scenarios, with a slightly higher fuel consumption. The reference tracking using the ideal power profile played a massive role in its effectiveness. In I, II, III and IV, although the ideal power profile was different than the actual profile at every instant, the general sense in its trend helped the control strategy work efficiently in real-time. In V, even though HMPC was still better than RB, the fuel consumption for HMPC increased because it kept trying to bring the battery SoC up to 0.65 once it went down, thereby making the fuel cell produce more power and consequently increasing the hydrogen consumption. In VI, the ideal power demand was the exact same as the actual power demand. Therefore, the reference values passed down from the upper level of HMPC was the globally optimized solution to the problem at the lower level. However, since the reference tracking was only a part of the objective function for the HMPC and the prediction horizon was small in comparison to the actual drive cycle time period, the fuel consumption was slightly more than the global minimum. The test cases V and VI is a clear indicator of HMPC's reference tracking capabilities.The rule-based control was the least effective of the three in all tested scenarios.

As was discussed in section 3.4, in a real situation, assuming the rule-based control as the worst case scenario, and the Quadratic programming problem as the benchmark, the Hierarchical MPC always fell between the two, with the results being closer to the globally optimized solution than the rule-based strategy.

6

Conclusion

This chapter gives a short conclusion to the study and addresses the research question that was formulated in chapter 1.

The literature review highlighted that Model Predictive Control is among the most effective energy management strategies for real-time applications. However, for vessels that do not operate under sustained high-load conditions where engines are already highly efficient, integrating MPC with hierarchical control presents a more practical and viable solution. The predictive capabilities of MPC, combined with the near-optimal reference values derived from the upper level of the hierarchical model, deliver superior performance.

In Chapter 3, the modelling of the powertrain for the H2C boat was addressed, focusing on the fuel cell and battery. Given the lack of detailed specifications, the modelling was approached with the necessity that the unspecified components could be scaled accordingly when required. Due to this limitation, a simplified state-space model was developed with the sole state of the system being the battery SoC. This parameter was crucial across all three controls for determining the power split between the fuel cell and the battery.

Chapter 4 detailed the creation of the three control strategies. The deterministic rule-based control was created to make decisions based on the battery SoC, instantaneous power demand, and the current behaviour of the system. Quadratic programming was used to minimize the hydrogen consumption, using the state-space model where the battery SoC served as the state variable and the power delivered by the fuel cell as the control variable. The power balance equation consisting of the battery power, fuel cell power, the power demand and the power losses integrated the model architecture into the state-space model. The mathematical framework of QP was used as the base for Hierarchical MPC formulation. In addition to the constraints and objectives of QP, reference tracking was implemented in HMPC, where a pre-solved QP problem (in its upper level) for an approximate power profile was used to guide the MPC (working at the lower level) towards the global optimal solution in real-time. However, real-world disturbances and uncertainties could deviate the HMPC solution from the theoretical global optimum.

Chapter 5 presented the testing process for QP and HMPC, which included parameter tuning, constraint feasibility tests and robustness tests. Finally, the results of comparing the control strategies were presented and interpreted. The parameter tuning focused on determining the optimal values of weights in the multi-criteria single-objective functions of both the QP and the HMPC, as well as identifying the best prediction horizon for running the HMPC. Feasibility tests for constraints confirmed that they were consistently obeyed and the objectives were achieved. Robustness tests assessed the system's tolerance to uncertainties in modeling and operational conditions, confirming that the system had a robust performance.

The research question introduced in this study at the beginning was:

"How efficiently can a Hierarchical MPC perform in real-time for the energy management of a hybrid marine powertrain?"

The focus of this question was on how effectively the strategy could reduce energy consumption, with hydrogen consumption serving as the key performance indicator. During the design phase of the controls, special consideration was given to ensure that the fuel cell operated as close to its maximum efficiency as possible when active.

To assess the competence of the HMPC, a comparative analysis framework was established. In this framework, the rule-based control strategy set the upper performance threshold, while Quadratic Programming acted as the benchmark. As expected, the performance of HMPC fell between the other two controls, with the rule-based control exhibiting the highest fuel consumption and QP achieving the lowest. The KPI for HMPC was notably closer to QP than to the rule-based control, indicating that HMPC's optimization solution was nearer to the global optimum. From the results, it could be concluded that the Hierarchical MPC operated with high efficiency for this system, effectively tracking the reference profile. Its prior knowledge of future trends in the power profile enhanced its optimality. The performance of the HMPC working with a complicated power profile in this study, reiterated this conclusion and the fact that it could work well with simpler profiles with lower power variations.

7

Recommendations and Future Work

The research done in this thesis utilized a simplified model of the powertrain. The focus was primarily on the battery and fuel cell while omitting the modelling of other components due to limited data availability. Even with the fuel cell and battery, not all their characteristics were considered. The thermal, fluidic, and chemical side of modelling were either excluded, simplified or linearized. Priority in this study was given to the development and testing of the Hierarchical MPC rather than achieving the most precise model. Since a PEM fuel cell can have about 11 or more states to develop just its state-space model[2], the complexity and detail required to build a very accurate model is immense. This research was focused more on the design, structure and mathematical verification phase of the controllers.

Future work could enhance the system's accuracy by incorporating more detailed models that include additional states, constraints, and refined objectives. This would increase the complexity of the system but would improve its alignment with real-world applications. They would eventually make it suitable for working well with the actual vessel. Scaling up the number of states and control variables would increase the computational complexity, but the general idea of the implementation of the control strategy remains unchallenged. Furthermore, future research could integrate component health as a KPI alongside fuel consumption. This approach would allow the controller to account for the degradation of the fuel cell, battery, or other components, potentially enhancing overall performance.

Although the Hierarchical MPC works well in comparison to QP and a rule-based controller, its capabilities have not been compared to other online real-time strategies. While the predictive nature of MPC usually provides better results in the long run, comparison of this control strategy to other optimization-based real-time strategies can help make it better. Instead of the worst-case scenario being the rule-based controller, the performance can be assessed with respect to better online optimization strategies. This could potentially help improve the comparitive framework further. Once the plant and the controller are more accurately designed, hardware-in-the-loop (HIL) testing could be conducted to evaluate the controller's performance with actual input-output components.

References

[1] Souleman M. Njoya, Olivier Tremblay, Louis-A Dessaint, et al. A generic fuel cell model for the simulation of fuel cell vehicles. In *2009 IEEE vehicle power and propulsion conference*, pages 1722–1729. IEEE, 2009.

[2] Guilherme Hideki Saito Diniz, Vinícius dos Santos Miranda, and Bruno Souza Carmo. Dynamic modelling, simulation, and control of hybrid power systems for escort tugs and shuttle tankers. *Journal of Energy Storage*, 72, 2023. ISSN 2352152X. doi: 10.1016/j.est.2023.108091.

[3] Huarong Zheng, Jun Wu, Weimin Wu, and Yuexuan Wang. Integrated motion and powertrain predictive control of intelligent fuel cell/battery hybrid vehicles. *IEEE Transactions on Industrial Informatics*, 16, 2020. ISSN 19410050. doi: 10.1109/TII.2019.2956209.

[4] Nikolaos Planakis, George Papalambrou, and Nikolaos Kyrtatos. Predictive control for a marine hybrid diesel-electric plant during transient operation. 2018. doi: 10.1109/CoDIT.2018.8394939.

[5] Nikolaos Planakis, Vasileios Karystinos, George Papalambrou, and Nikolaos Kyrtatos. Transient energy management controller for hybrid diesel-electric marine propulsion plants using nonlinear mpc. volume 53, 2020. doi: 10.1016/j.ifacol.2020.12.1837.

[6] Stephanie Stockar, Vincenzo Marano, Giorgio Rizzoni, and Lino Guzzella. Optimal control for plug-in hybrid electric vehicle applications. 2010. doi: 10.1109/acc.2010.5530752. - see refs 13 and 20 for more info on PMP.

[7] Georgios Papalambrou, Sergey Samokhin, Sotirios Topaloglou, Nikolaos Planakis, Nikolaos Kyrtatos, and Kai Zenger. Model predictive control for hybrid diesel-electric marine propulsion. volume 50, 2017. doi: 10.1016/j.ifacol.2017.08.2488. -MPC and Adaptive MPC used.

[8] Nikolaos Planakis, George Papalambrou, and Nikolaos Kyrtatos. A real-time power-split strategy for a hybrid marine power plant using mpc. *International Journal of Modelling, Identification and Control*, 34, 2020. ISSN 17466180. doi: 10.1504/IJMIC.2020.110350.

[9] Jihun Han, Antonio Sciarretta, and Nicolas Petit. Handling state constraints in fast-computing optimal control for hybrid powertrains. volume 50, 2017. doi: 10.1016/j.ifacol.2017.08.961.

[10] Lin He, Tielong Shen, Liangyao Yu, Nenglian Feng, and Jian Song. A model-predictive-control-based torque demand control approach for parallel hybrid powertrains. *IEEE Transactions on Vehicular Technology*, 62:1041–1052, 3 2013. ISSN 0018-9545. doi: 10.1109/TVT.2012.2218291. URL `http://ieeexplore.ieee.org/document/6298983/`.

[11] Dominique Van Mullem, Thijs Van Keulen, John Kessels, Bram De Jager, and Maarten Steinbuch. Implementation of an optimal control energy management strategy in a hybrid truck. volume 43, 2010. doi: 10.3182/20100712-3-DE-2013.00067.

[12] Abdel Ra ouf Mayyas, Sushil Kumar, Pierluigi Pisu, Jacqueline Rios, and Puneet Jethani. Model-based design validation for advanced energy management strategies for electrified hybrid power trains using innovative vehicle hardware in the loop (vhil) approach. *Applied Energy*, 204, 2017. ISSN 03062619. doi: 10.1016/j.apenergy.2017.07.028.

[13] Pier Giuseppe Anselma, Yi Huo, Joel Roeleveld, Giovanni Belingardi, and Ali Emadi. Slope-weighted energy-based rapid control analysis for hybrid electric vehicles. *IEEE Transactions on Vehicular Technology*, 68, 2019. ISSN 19399359. doi: 10.1109/TVT.2019.2899360.

[14] Lucas Bruck and Ali Emadi. A new regen-based energy management strategy for online control of hybrid powertrains. pages 762–766. IEEE, 6 2021. ISBN 978-1-7281-7583-6. doi: 10.1109/ITEC51675.2021.9490092. URL `https://ieeexplore.ieee.org/document/9490092/`.

[15] Alberto Broatch, Pablo Olmeda, Benjamín Plá, and Amin Dreif. Novel energy management control strategy for improving efficiency in hybrid powertrains. *Energies*, 16, 2023. ISSN 19961073. doi: 10.3390/en16010107.

[16] Chao Xu, Liyun Fan, Yongming Feng, Yuanqing Zhu, Chongchong Shen, and Zejun Jiang. A multi-objective optimization energy management strategy for marine hybrid propulsion with waste heat recovery system. *Applied Thermal Engineering*, 236, 2024. ISSN 13594311. doi: 10.1016/j.applthermaleng.2023.121548.

[17] Nikolaos Planakis, George Papalambrou, and Nikolaos Kyrtatos. Ship energy management system development and experimental evaluation utilizing marine loading cycles based on machine learning techniques. *Applied Energy*, 307, 2022. ISSN 03062619. doi: 10.1016/j.apenergy.2021.118085.

[18] D. Pivetta, C. Dall'Armi, and R. Taccani. Multi-objective optimization of hybrid pemfc/li-ion battery propulsion systems for small and medium size ferries. *International Journal of Hydrogen Energy*, 46, 2021. ISSN 03603199. doi: 10.1016/j.ijhydene.2021.02.124.

[19] Hegazy Rezk, Ahmed M. Nassef, Mohammad Ali Abdelkareem, Abdul Hai Alami, and Ahmed Fathy. Comparison among various energy management strategies for reducing hydrogen consumption in a hybrid fuel cell/supercapacitor/battery system. *International Journal of Hydrogen Energy*, 46, 2021. ISSN 03603199. doi: 10.1016/j.ijhydene.2019.11.195.

[20] Mingliang Bai, Wenjiang Yang, Ruopu Zhang, Marek Kosuda, Peter Korba, and Michal Hovanec. Fuzzy-based optimal energy management strategy of series hybrid-electric propulsion system for uavs. *Journal of Energy Storage*, 68, 2023. ISSN 2352152X. doi: 10.1016/j.est.2023.107712.

[21] Ye Xie, Shaoming He, Al Savvaris, Antonios Tsourdos, Dan Zhang, and Anhuan Xie. Convexification in energy optimization of a hybrid electric propulsion system for aerial vehicles. *Aerospace Science and Technology*, 123, 2022. ISSN 12709638. doi: 10.1016/j.ast.2022.107509.

[22] Jianyun Zhu, Li Chen, Bin Wang, and Lijuan Xia. Optimal design of a hybrid electric propulsive system for an anchor handling tug supply vessel. *Applied Energy*, 226, 2018. ISSN 03062619. doi: 10.1016/j.apenergy.2018.05.131.

[23] Haowen Hu, Wei Wei Yuan, Minghang Su, and Kai Ou. Optimizing fuel economy and durability of hybrid fuel cell electric vehicles using deep reinforcement learning-based energy management systems. *Energy Conversion and Management*, 291, 2023. ISSN 01968904. doi: 10.1016/j.enconman.2023.117288.

[24] Robert Luca, Michael Whiteley, Toby Neville, Paul R. Shearing, and Dan J.L. Brett. Comparative study of energy management systems for a hybrid fuel cell electric vehicle - a novel mutative fuzzy logic controller to prolong fuel cell lifetime. *International Journal of Hydrogen Energy*, 47, 2022. ISSN 03603199. doi: 10.1016/j.ijhydene.2022.05.192.

[25] Teresa Donateo, Claudia Lucia De Pascalis, Luciano Strafella, and Antonio Ficarella. Off-line and on-line optimization of the energy management strategy in a hybrid electric helicopter for urban air-mobility. *Aerospace Science and Technology*, 113, 2021. ISSN 12709638. doi: 10.1016/j.ast.2021.106677.

[26] Li Chen, Huachao Dong, and Zuomin Dong. Integrated system design and control optimization of hybrid electric propulsion system using a bi-level, nested approach. volume 2A-2019, 2019. doi: 10.1115/DETC2019-97456.

[27] Sebastien Delprat, Jimmy Lauber, Thierry Marie Guerra, and J. Rimaux. Control of a parallel hybrid powertrain: Optimal control. *IEEE Transactions on Vehicular Technology*, 53, 2004. ISSN 00189545. doi: 10.1109/TVT.2004.827161.

[28] Xiaohui Zhang, Li Liu, and Yueling Dai. Fuzzy state machine energy management strategy for hybrid electric uavs with pv/fuel cell/battery power system. *International Journal of Aerospace Engineering*, 2018, 2018. ISSN 16875974. doi: 10.1155/2018/2852941.

[29] Tao LEI, Zhou YANG, Zicun LIN, and Xiaobin ZHANG. State of art on energy management strategy for hybrid-powered unmanned aerial vehicle, 6 2019. ISSN 10009361.

[30] Huiying Liu, Yongming Yao, Jie Wang, Yutong Qin, and Tianyu Li. A control architecture to coordinate energy management with trajectory tracking control for fuel cell/battery hybrid unmanned aerial vehicles. *International Journal of Hydrogen Energy*, 47:15236–15253, 4 2022. ISSN 03603199. doi: 10.1016/j.ijhydene.2022.03.036.

[31] Sailing Innovation Centre. H2c boat. URL https://www.sailinginnovationcentre.nl/h2c-boat/.

[32] Torqeedo. Battery and motor technology. URL https://www.torqeedo.com/en/green-propulsion/battery-technology-com.html#db40.

[33] A. Albarbar and M. Alrweq. *Proton Exchange Membrane fuel cells: Design, Modelling and performance assessment techniques*. Springer, Switzerland, 2018.

[34] S.V. Puranik, A. Keyhani, and F. Khorrami. State-space modelling of proton exchange membrane fuel cell. *IEEE Transactions on Energy Conversion*, 25(3):804–812, 2010.

[35] Qian Xun, Yujing Liu, Jian Zhao, and Emma Arfa Grunditz. Modelling and simulation of fuel cell/supercapacitor passive hybrid vehicle system. In *2019 IEEE Energy Conversion Congress and Exposition (ECCE)*, pages 2690–2696. IEEE, 2019.

[36] Mohsen Banaei, Mehdi Rafiei, Jalil Boudjadar, and Mohammad-Hassan Khooban. A comparative analysis of optimal operation scenarios in hybrid emission-free ferry ships. *IEEE Transactions on Transportation Electrification*, 6(1):318–333, 2020.

[37] Dan Deng, Jialu Qiao, Jun Qi, Shunli Wang, Siyu Jin, Xianyong Xiao, Xueyi Hao, and Yunlong Shang. Chapter 6 - equivalent modeling and parameter identification of power lithium-ion batteries. In Shunli Wang, Kailong Liu, Yujie Wang, Daniel-Ioan Stroe, Carlos Fernandez, and Josep M. Guerrero, editors, *State Estimation Strategies in Lithium-ion Battery Management Systems*, pages 95–124. Elsevier, 2023. ISBN 978-0-443-16160-5. doi: https://doi.org/10.1016/B978-0-443-16160-5.00001-9. URL https://www.sciencedirect.com/science/article/pii/B9780443161605000019.

[38] Xuezhou Wang, Udai Shipurkar, Ali Haseltalab, Henk Polinder, Frans Claeys, and Rudy R Negenborn. Sizing and control of a hybrid ship propulsion system using multi-objective double-layer optimization. *Ieee Access*, 9:72587–72601, 2021.

[39] Nick Gould and Philippe L Toint. Preprocessing for quadratic programming. *Mathematical Programming*, 100:95–132, 2004.

[40] Jianyun Zhu, Li Chen, Bin Wang, and Lijuan Xia. Optimal design of a hybrid electric propulsive system for an anchor handling tug supply vessel. *Applied energy*, 226:423–436, 2018.

[41] Alberto Bemporad and Manfred Morari. Robust model predictive control: A survey. In *Robustness in identification and control*, pages 207–226. Springer, 2007.

Energy Management Strategies for Hybrid Marine Powertrains

Siddharth Sasidharan[1] and Dr. Andrea Coraddu[2]

Abstract— **Reduction of carbon emissions and greenhouse gases within the transportation sector is crucial due to its significant contribution to environmental degradation. To reduce this impact, it is important to develop and implement energy efficient systems. In addition to exploring renewable fuel alternatives, effective energy management systems are vital. This paper presents an optimization-based control referred to as Hierarchical Model Predictive Control along with a comparitive framework, to evaluate its effectiveness as a real-time control strategy. Three energy management strategies are designed for this purpose, with the objective of minimizing the fuel consumption of a hybrid marine powertrain, while optimizing the power distribution among its components to achieve high operational efficiency.**

I. INTRODUCTION

The transportation sector contributes approximately 30 % to the total global greenhouse gas (GHG) emissions [1]. Recognizing this issue, the International Maritime Organization (IMO) has proposed a strategic plan aimed at achieving a 40 % reduction in GHG emissions by 2030 and a net-zero emission target by 2050 in the maritime sector [2]. Although electric and hybrid propulsion technologies hold great promise in meeting these emission targets, significant obstacles remain, especially in improving fuel efficiency, optimizing energy storage systems, and perfecting energy conversion processes between subsystems. Fuel cell-powered hybrid powertrains have emerged as a good alternative, which couples electric propulsion driven by a fuel-cell system with an auxiliary battery. This configuration not only achieves substantial emission reductions, but also minimizes environmental impact, with water and heat being the primary by-products of the propulsion process.

Hybrid powertrain architectures vary depending on how energy contributions from different sources are managed. As a result, optimizing energy management has become a central focus in recent years. This has led to significant scholarly attention on Energy Management Systems (EMS) for hybrid powertrains across the automotive, marine, and aviation sectors.

While the primary aim of most EMSs is to minimize fuel consumption, these strategies often address additional objectives, such as optimizing the sizing of key powertrain components, mitigating battery degradation, and reducing pollutants and emissions. EMSs are generally classified into offline and real-time strategies based on their computational demands, implementation timing with respect to the plant being controlled, and the optimality of their solutions.

Offline strategies optimize energy management using prior knowledge of the drive cycle and relevant energy variables' trajectories (such as speed, torque or power) to deliver global optimal solutions. They often serve as benchmarks, form part of a multi-level EMS, or act as the foundation for online (real-time) EMS development. Due to the availability of prior knowledge, offline strategies provide globally optimized solutions, offering the best possible outcome for a given situation. This helps in using it as a benchmark for comparing other control strategies [3], [4], [5], [6], [7], [8]. The offline strategies have also often been used as the part of a bigger system. They act as optimizers at the cloud level, providing information and data for a real-time control at the lower level. The computational complexity of the global optimization is thus surpassed [9], [10]. They have also been used as a foundation for developing real-time strategies. For example, the offline control strategy based on Pontryagin's Minimum Principle [11] is used to develop the Equivalent Consumption Minimization Strategy (ECMS), which functions as a real-time control strategy.

Real-time strategies are characterized by their simplicity, reduced computation time, predictive capabilities, and instantaneous implementation. The issue, however, is that they can only provide sub-optimal solutions and cannot reach global optimality. These strategies can be broadly classified into rule-based, online optimization-based, and learning-based control strategies. Rule-based strategies are based on precalculated rules that cannot be altered or reprogrammed during operation without human intervention [12]. They may use deterministic or fuzzy rules, or utilize look-up tables. Owing to their simplicity, Rule-based (RB) EMSs can be implemented in real-time. However, they have several drawbacks, the most significant being their inability to provide optimal solutions. In real-time optimization methods, the control variable is determined by minimizing a predefined cost function based on future equivalence assumption of the electric energy consumption [13]. The most widely used strategies in this category are ECMS (Equivalent Consumption Minimisation Strategy) and MPC (Model Predictive Control). In a Learning-based EMS, the necessity for precise model information diminishes, as control decisions are made based on learning through interactions with the environment. A reinforcement learning (RL) system consists of a learning agent and studies its interaction with the environment. At each time step, the learning agent receives an observation of the environment, selects an action based on the observed state, transitions to a new state as a result of the action, and

[1]Siddharth Sasidharan is with Faculty of Mechanical Engineering, Delft University of Technology, Mekelweg 2, 2628 CD Delft, The Netherlands

[2]Dr. Andrea Coraddu is an Associate Professor with the Faculty of Mechanical Engineering, Delft University of Technology, Mekelweg 2, 2628 CD Delft, The Netherlands

then computes the reward associated with the transition. This reward is then provided as a feedback to the learning agent. Over time, through the iterative process, the optimal policy can guide the learning agent to take the best series of actions to maximise the cumulated reward.

This paper focuses on creating a Hierarchical-MPC, which operates in real time and can provide solutions that are close to global optimality. Additionally, a comparitive framework is created using a rule-based control and quadratic programming. Since rule-based control strategies cannot provide optimal solutions, they can serve as an upper bound in minimization control problems for real-time strategies, which should not be easily surpassed. Quadratic programming, the offline optimization strategy, is used both as benchmark for Hierarchical MPC and as a foundation for its development. This allows for a comprehensive comparison to assess the competence of the Hierarchical MPC.

The structure of the paper is as follows: Section II presents the description and mathematical modelling of the plant. In section III, the three EMSs are developed and their mathematical formulations are discussed. Following this, in Section IV, the specifications of the three control strategies for this specific system are defined, and they are compared. Finally, Section V concludes this paper.

II. MATHEMATICAL MODELLING

The marine vessel utilized in this research is an H2C boat, a hydrogen-powered rigid-hull inflatable boat (RIB or RHIB) with a hull made of either polyester or aluminium [14]. Such boats are typically equipped with powerful onboard engines. This particular vessel is powered by a combination of hydrogen fuel cells and lithium-ion batteries. The architecture of the powertrain follows a parallel configuration as illustrated in Figure 1. In this setup, energy flows unidirectionally from the fuel cell to the DC converters, while the battery features a bidirectional energy flow to support both charging and discharging of the lithium-ion batteries.

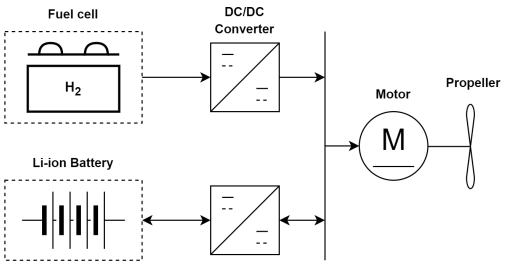

Fig. 1. Powertrain architecture of boat

A 'Deep Blue' electric drive system from the company Torqeedo [15] is used on the boat. The Lithium-ion battery has a usable capacity of 38 kWh with a 2 kWh reserve, a nominal voltage of 360 V, and can deliver a continuous maximum power of 55 kW. Fuel cell serves as a range extender. A low-temperature proton-exchange membrane fuel cell (LT-PEMFC) is used, that can deliver a maximum power of 50 kW.

A. Fuel cell

The detailed model of the LT-PEMFC used here is based on the works of Njoya et. al [16] and Xun et al. [17]. It considers parameters such as pressures, temperature, compositions, and flow rates of fuel and air. Considering the kinetics of the reactions taking place at the electrodes and inside, the fuel cell voltage can be given as follows:

$$V_{fc} = E_{oc} - V_{act} - I_{fc}R_{ohm} \tag{1}$$

$$E_{oc} = NK_cE_n \tag{2}$$

$$V_{act} = NA\ln\left[\frac{I_{fc}}{I_0}\right] \cdot \frac{1}{sT_d/3+1} \tag{3}$$

where E_{oc} is the open circuit voltage (V), V_{act} is the voltage due to activation losses (V), I_{fc} is the fuel cell current (A), R_{ohm} is the internal resistance (Ω), N is the number of cells, K_c is the voltage constant at nominal condition of operation, A is the Tafel slope (V), I_0 is the exchange current (A), and T_d is the stack settling time or response time (at 95% of the final value). The activation losses, which characterises the delayed response due to the rate of chemical reactions at the electrode surfaces, is represented by the first order transfer function $\frac{1}{sT_d/3+1}$, with s being the frequency variable in the Laplace domain.

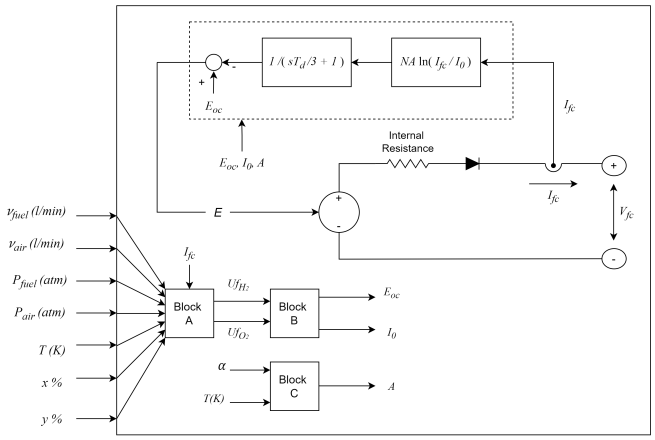

Fig. 2. Detailed fuel cell stack model replicating the work of [16]

The model is illustrated in detail in the Figure 2. Using the blocks A, B and C, where E_{oc}, I_0 and A are updated based on the varying parameters ν_{fuel} (fuel flow rate in litres/min), ν_{air} (air flow rate in litres/min), P_{fuel} (absolute supply pressure of fuel in atm), P_{air} (absolute supply pressure of air in atm), T, $x\%$ (percentage of hydrogen in the fuel) and $y\%$ (percentage of oxygen in the oxidant) . Using these inputs into Block A, the rate of utilization of hydrogen and oxygen are calculated as follows:

$$Uf_{H_2} = \frac{60000RTI_{fc}}{zFP_{fuel}\nu_{fuel}x\%} \tag{4}$$

$$Uf_{O_2} = \frac{60000RTI_{fc}}{2zFP_{air}\nu_{air}y\%} \tag{5}$$

In the block B, to calculate the Nernst voltage and exchange current, the partial pressures are computed as follows:

$$P_{H_2} = (1 - Uf_{H_2})x\%P_{fuel} \tag{6}$$

$$P_{O_2} = (1 - Uf_{O_2})y\%P_{air} \tag{7}$$

$$P_{H_2O} = (w + 2y\%Uf_{O_2})P_{air} \tag{8}$$

In the Nernst equation, P_{H_2O} becomes 1 if T¡373K. Finally, using the values of partial pressures and the Nernst voltage, block B and C computes I_0 and A as follows:

$$I_0 = \frac{zFk\left(P_{H_2} + P_{O_2}\right)}{Rh} \cdot \exp\left(\frac{-\Delta G}{RT}\right) \tag{9}$$

$$A = \frac{RT}{z\alpha F} \tag{10}$$

where k is the Boltzmann's constant (1.38×10^{-23} J/K) and h is the Planck's constant (6.626×10^{-34} Js).

While the fuel cell can provide reliable power at steady state conditions, some of the power it generates is wasted and cannot be delivered to the load due to activation losses, ohmic losses, mass transfer or concentration losses, and thermal losses. Based on the fuel cell power-efficiency relationship seen in Banaei et al.[18], these losses vary with the power generated by the fuel cell. Using the data derived from that relationship and by curve fitting, the relationship between the normalized values of generated power and the actual power output is established as a quadratic function, given by:

$$\frac{P_{fc_{gen}}}{k_{fc}} = 0.9131 \cdot \left(\frac{P_{fc_{out}}}{k_{fc}}\right)^2 + 0.8451 \cdot \left(\frac{P_{fc_{out}}}{k_{fc}}\right) + 0.0700 \tag{11}$$

where,

$$P_{fc_{gen}} = E_{oc} \cdot I_{fc} \tag{12}$$

and k_{fc} is the maximum rated power output of the fuel cell, considering all the losses.

The KPI used for analysing and comparing the control strategies is hydrogen consumption. To calculate the instantaneous hydrogen consumption, the following relation is used:

$$m_{H_2}(t) = P_{fc_{gen}}(t) \cdot \Delta t \cdot \mu \tag{13}$$

where m_{H_2} (kg) is the mass of hydrogen consumed and μ (kg/kWh) is the reciprocal of usable energy of Hydrogen.

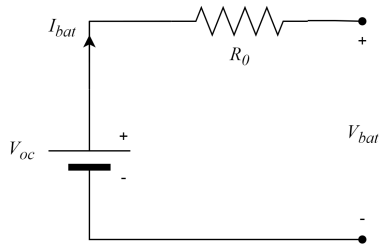

Fig. 3. Rint equivalent circuit model

B. Battery

To accurately model the working characteristics of this battery, an equivalent circuit modelling concept is used. Commonly used models include the Rint and Thevenin models. While the Thevenin model accounts for the polarization effects of the lithium-ion battery and provides a more precise behavioural representation, this research utilizes the Rint model due to its computational simplicity.

The Equivalent circuit consists of an ideal voltage source and a resistance R_0, as illustrated in the Figure 3. The resistance R_0 characterizes the internal ohmic resistance of the battery. Using Kirchoff's law, we obtain the relation:

$$V_{bat} = V_{oc} - I_{bat}R_0 \tag{14}$$

where V_{oc} is the battery's open circuit voltage (which assumed to be a constant) and I_{bat} is the current flowing through the circuit.

The only loss in power in this scenario is due to the internal resistance. The power drawn and the power losses from the battery can thus be defined as follows:

$$P_{bat} = V_{oc}I_{bat} \tag{15}$$

$$P_{loss} = I_{bat}^2 R_0 \tag{16}$$

An important property of the battery on which its performance depends is the State of Charge (SoC). It is a unitless quantity which represents the remaining useful charge inside the battery and can be expressed as follows [19]:

$$SoC(t + \Delta t) = SoC(t) - \frac{P_{bat}(t) \cdot \Delta t}{E_{bat}} \tag{17}$$

where E_{bat} is the energy rating of the battery.

III. ENERGY MANAGEMENT SYSTEMS

Three distinct control strategies are developed for managing energy and power distribution among the power sources of the H2C boat: Rule-Based (RB) Control, Global Optimization using Quadratic Programming (QP), and Hierarchical Model Predictive Control (HMPC). QP is chosen for its similarity to classical Model Predictive Control (MPC) in formulation and structure. The Rule-based control and HMPC work in real-time, while the QP is an offline control strategy. The RB and QP strategies are implemented to

compare performance and assess the potential of the HMPC. All three strategies are designed to adhere to the following core principles:

- Minimize hydrogen use
- When the fuel cell is in operation, maximize its efficiency, which inadvertently means operating the fuel cell at or near its optimal power output, $P_{optimal}$
- Always meet the power demand
- Maintain the battery SoC within limits, in the range $[SoC_{min}, SoC_{max}]$. This helps with reducing battery degradation.
- Use battery to absorb sudden changes in power demand, while the fuel cell's power output should be kept as stable as possible. The rate of change of P_{fc} is limited to $[-\epsilon, \epsilon]$

A. Rule-based Control

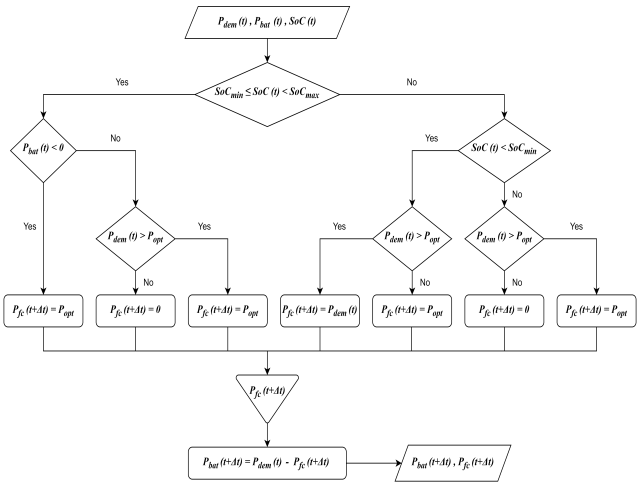

Fig. 4. Flow chart for the Rule-based control

As illustrated in Figure 4, the rule-based control is designed with three inputs and two outputs. It operates in the discrete time domain. P_{bat}, the power consumed or delivered by the battery in the current time-step is used as an input, to help stabilise the system behaviour with regards to being consistent with the battery modes. A negative value of P_{bat} indicates charging, and positive value indicates the discharging mode. The other two inputs are the power demand for the upcoming time-step and the battery state of charge of the current time-step. The outputs are the fuel cell power and battery power requested for the next time-step.

The control strategy first compares the SoC at that instant to its allowable range. If it is in the within the range $[SoC_{min}, SoC_{max})$, it looks into whether the battery was charging or discharging at that instant, and then makes a decision considering the power demand. If the SoC is below SoC_{min}, the battery is charged unless the power demand is greater than the optimal power output of the fuel cell. However, if the SoC is greater than or equal to SoC_{max}, the power demand is satisfied by the battery as long as its below P_{opt}. If the demand is more, the power is split among the power sources.

B. Quadratic Programming

The Quadratic Programming problem defined below is a multi-criteria single-objective optimization problem where the cost function has two main goals. The first weighted part of this objective function minimizes the normalized fuel cell power or the control variable over the entire power profile, thereby reducing the total fuel consumption. This is given a weighting factor of ω_1. The second part tries to minimize the error between power produced by the fuel cell at any instant and the optimal fuel cell power $P_{optimal}$. Reducing this error helps the fuel cell to run at its maximum efficiency. The weighting factor ω_2 is determined such that this part of the objective function is active when $u_{fc} > 0$, i.e., when the fuel cell is turned on. To keep the priorities of the objectives consistent with each other, all the terms are normalized.

Minimize

$$J = \sum_{i=1}^{N} [\omega_1 \cdot u_{fc}(i) + \omega_2 \cdot \left(u_{fc}(i) - \frac{P_{optimal}}{k_{fc}} \right)^2]$$

subject to:

$$SoC(i+1) = SoC(i) + \frac{k_{fc} \cdot \tau_s \cdot u_{fc}(i)}{E_{bat}} - \frac{[P_{dem}(i) + P_{loss}(i) + P_d(i)] \cdot \tau_s}{E_{bat}} \tag{18}$$

$$y(i) = SoC(i) \tag{19}$$

$$SoC_{min} \leq SoC(i) \leq SoC_{max} \tag{20}$$

$$0 \leq u_{fc}(i) \leq 1 \tag{21}$$

$$P_{bat} = P_{dem}(i) + P_{loss}(i) + P_d(i) - (k_{fc} \cdot u_{fc}(i)) \tag{22}$$

$$-1 \leq \left[\frac{P_{bat}(i)}{k_{bat}} \right] \leq 1 \tag{23}$$

$$\frac{-\epsilon}{k_{fc}} \leq [u_{fc}(i+1) - u_{fc}(i)] \leq \frac{\epsilon}{k_{fc}} \tag{24}$$

$$\forall i \in [1, N]$$

The problem is subject to multiple constraints, which describe the behaviour of the system. The first two constraints are the state-space equations, describing the system dynamics. Equation (20) limits the range of the battery state of charge to $[SoC_{min}, SoC_{max}]$. Equation (21) restricts u_{fc} to the range [0,1], and consequently constrains the output power of the fuel cell to stay within its operational range. Similarly, Equation (23) limits the power produced by the battery to the range [$-k_{bat}$,k_{bat}], where k_{bat} is the maximum power that can be produced by the battery. The

final constraint, Equation (24), limits the rate of change of the power output of fuel cell. This ensures that significant power variations are handled by the battery and not the fuel cell. The absolute value of change in u_{fc} in the sampling time is limited to ϵ.

C. Hierarchical Model Predictive Control

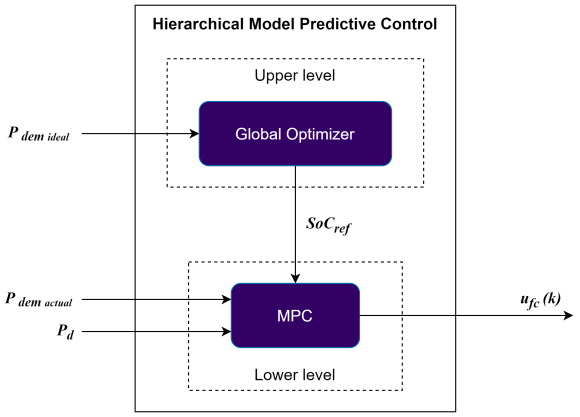

Fig. 5. Hierarchical MPC

The Hierarchical Model Predictive Control (HMPC) functions similarly to classical MPC by performing real-time optimization over a prediction horizon. As shown in Figure 5, the reference values for the battery state of charge is obtained from the upper level. These values are the results of global optimization, which in this case is a Quadratic Programming problem, done prior to the operation of the vessel. An ideal power profile, which anticipates the upcoming drive cycle of the boat, is made available to the global optimizer as an exogenous input, and the problem is then optimized over the entire period of operation. These globally optimized reference values for the SoC are subsequently passed to the HMPC, where they serve as targets during the vessel's real-time operation. The HMPC continually compares the real-time system behavior with these reference values and adjusts the power split between the fuel cell and the battery accordingly. The mathematical formulation of the control problem is defined as follows:

Minimize

$$J = \sum_{i=0}^{N_p} [\omega_1 \cdot u_{fc}(k+i) + \omega_2 \cdot \left(u_{fc}(k+i) - \frac{P_{optimal}}{k_{fc}} \right)^2 + \omega_3 \cdot (SoC(k+i) - SoC_{ref}(k+i))^2]$$

subject to:

$$SoC(k+i+1) = SoC(k+i) + \frac{k_{fc} \cdot u_{fc}(k+i) \cdot \tau_s}{E_{bat}} - \frac{(P_{dem}(k+i) + P_{loss}(k+i) + P_d(k+i)) \cdot \tau_s}{E_{bat}} \quad (25)$$

$$y(k+i) = SoC(k+i) \quad (26)$$

$$SoC_{min} \leq SoC(k+i) \leq SoC_{max} \quad (27)$$

$$0 \leq u_{fc}(k+i) \leq 1 \quad (28)$$

$$P_{bat}(k+i) = P_{dem}(k+i) + P_{loss}(k+i) + P_d(k+i) - (k_{fc} \cdot u_{fc}(k+i)) \quad (29)$$

$$-1 \leq \left[\frac{P_{bat}(k+i)}{k_{bat}} \right] \leq 1 \quad (30)$$

$$\frac{-\epsilon}{k_{fc}} \leq [u_{fc}(k+i) - u_{fc}(k+i-1)] \leq \frac{\epsilon}{k_{fc}} \quad (31)$$

$$\forall i \in [0, N_p]$$

The objective function of the HMPC focuses on three key aspects: minimizing fuel consumption, ensuring the fuel cell operates at its optimal power, and reducing the error between the actual battery SoC and the reference SoC value obtained from the Quadratic Programming problem in the upper level. These are prioritized by using the weights ω_1, ω_2 and ω_3 respectively. In addition to the first two terms of the objective function similar to the QP problem, $\omega_3 \cdot (SoC(k+i) - SoC_{ref}(k+i))^2$ minimizes the error between the actual SoC and the reference SoC over the horizon to keep the system aligned with the global optimizer's target and follow its path. k is the time-step during the optimization and i denotes the horizon steps.

The upper-level global optimization does not consider the disturbances (winds or waves) or changes in physical characteristics of the system (such as additional cargo or people onboard the vessel) which is not known beforehand. However, the HMPC, working in real-time, adjusts for these disturbances faced by the system, while still meeting the actual power demands. From the reference tracking, it gets a general idea of what it can expect in the near future. This helps it choose when to switch on the fuel cell and when to turn it off with minimal variations in its power production.

IV. RESULTS

A. Objective Function Weights

The weights used in the objective function of the optimization strategies are crucial for managing the desired behavior of the controls. A Grid Search method is employed to adjust the weights of the multiple criteria in the objective function. Using the concept of Grid search, the weights (ω) assumed by the multiple criteria in the objective function are selected by discretizing the range [0,1] into a number of partitions of equal equal gap between them. This allows for systematic testing of different values to find the most optimal ω values. For the Quadratic Programming (QP) strategy, the optimal values for ω_1 and ω_2 are determined in this way. The weights ω_1 and ω_2 are defined such that their sum always equals to 1. In the Hierarchical MPC (HMPC), for simplicity and to maintain consistency, the ratio between ω_1 and ω_2 from the QP is preserved, while the optimal value for ω_3 is tuned with

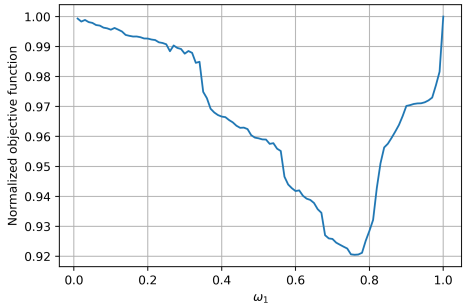

Fig. 6. Grid search for ω determination in QP

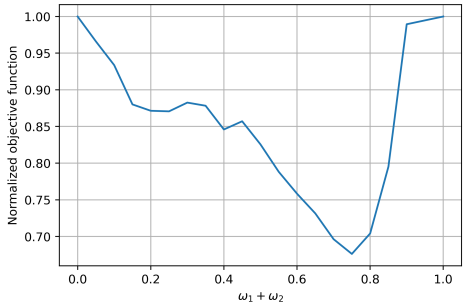

Fig. 7. Grid search for ω determination in HMPC

respect to the first two weights. All three weights add up to 1 too.

In this Grid-search approach, the weights are systematically varied from 0 to 1, the optimization problem is solved for each set of values, and the corresponding normalized objective function is calculated. Since this is a multi-criteria single objective minimization problem, the weight combination that yields the lowest value of the objective function is selected as optimal.

As can be seen in the Figure 6, for the objective function of QP, the values for ω_1 and ω_2 are 0.78 and 0.22. From the minimum of the normalized objective function in Figure 7, it can be seen that the optimal values for ω_1, ω_2 and ω_3 in HMPC are 0.585, 0.165 and 0.25 respectively.

B. Prediction Horizon

Identifying the prediction horizon, N_p for the HMPC involves balancing fuel consumption and computational complexity. As N_p increases, the computational time and complexity of the HMPC optimization problem increase.

From Figure 8, it is clear that increase in N_p leads to better optimization results. However, after a certain point, which in this case is an N_p of 80 seconds, the fuel consumption started to converge, and further increases in the prediction horizon do not result in significant reductions in fuel consumption. Therefore, a value of 80 seconds was taken as the optimal value of N_p for this case.

C. Control Strategy Comparison

Multiple profiles were run for comparing the control strategies with varying levels of prior knowledge, as given

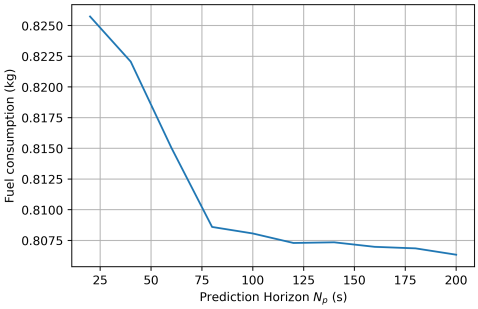

Fig. 8. Test for N_p determination

in Table I. For the first four scenarios, an actual power profile obtained from running the H2C boat was used as the ideal demand power. To simulate real-world conditions, the disturbances or variations in this power demand were introduced to this profile to obtain the actual power demand. This added disturbance was a stochastic variable with varying ranges of power from the ideal profile, with the condition that the actual power demand as such does not take a negative value. In the first four power profiles, the only difference was thus the variation in P_d, quantified as a random variable with an allowable range of $[-0.2P_{dem_{max}}, 0.2P_{dem_{max}}]$. In the fifth case, the power profile was the same as the fourth, but the reference values obtained from the upper level of HMPC (SoC reference values) were kept constant at 0.65. In the sixth case, the actual power profile was set the same as the ideal profile (with $P_d = 0$).

Test case	**Fuel consumption (kg)**		
	RB control	**HMPC**	**QP**
I	1.1143	0.8067	0.7628
II	0.9912	0.8232	0.7344
III	1.0510	0.8197	0.7476
IV	1.1202	0.8303	0.7660
V	1.1202	0.9156	0.7660
VI	0.9794	0.7002	0.6915

TABLE I
CONTROL STRATEGY COMPARISON

The offline control strategy performed the best, providing a globally optimized solution to the control problem. The total hydrogen consumption over the entire drive cycle was minimized while simultaneously keeping the power generation of the fuel cell at the most efficient point as much as possible.

The Hierarchical MPC had comparable results to QP in the

first four scenarios, although always having slightly higher fuel consumption. The reference tracking of the ideal power profile played a massive role in its effectiveness. In I, II, III and IV, although the ideal power profile is different than the actual profile at every instant, the general sense of change in the profile helped it work efficiently in real-time. In V, even though HMPC was still better than RB, the fuel consumption for HMPC increased because it kept trying to bring the battery SoC up to 0.65 once it went down, thereby making the fuel cell produce more power and consequently increasing the Hydrogen consumption. In VI, the ideal power demand was the exact same as the actual power demand. Therefore, the reference values passed down from the upper level of HMPC was the globally optimized solution to the problem at the lower level. Thus, since the reference tracking is only a part of the objective function for the HMPC, the fuel consumption was very close to the global optimum, but still slightly more due to the effect of smaller prediction horizon in comparison to the actual drive cycle time period.

The rule-based control had the highest hydorgen consumption of the three in all scenarios and acted as the upper bound for the solutions.

V. CONCLUSION

This paper was focused on how much the HMPC strategy could reduce the energy consumption, KPI being hydrogen consumption. It was also considered during the creation of the control strategies that the fuel cell needed to operate as close to conditions of maximum efficiency as possible, when it was turned on. To assess the capabilities of the HMPC, a comparative analysis framework was established. In this framework, the rule-based control strategy served as the upper threshold and Quadratic Programming served as the benchmark. As expected, the performance of HMPC fell between the other two, with the KPI of HMPC being closer to that of QP than the rule-based. It is evident that the solution to the optimization problem provided by HMPC was closer to the global optimum. It is able to track the reference profile effectively. This knowledge of the future trend in the power profile enhances its ability to obtain near-optimal solutions.

REFERENCES

[1] H. Zheng, J. Wu, W. Wu, Y. Wang, Integrated motion and powertrain predictive control of intelligent fuel cell/battery hybrid vehicles. IEEE Transactions on Industrial Informatics, 16, 2020. ISSN 19410050. doi: 10.1109/TII.2019.2956209.

[2] N. Planakis, G. Papalambrou, N. Kyrtatos, Predictive control for a marine hybrid diesel-electric plant during transient operation. 2018. doi:10.1109/CoDIT.2018.8394939.

[3] J. Han, A. Sciarretta, N. Petit, Handling state constraints in fast-computing optimal control for hybrid powertrains. volume 50, 2017. doi: 10.1016/j.ifacol.2017.08.961.

[4] L. He, T. Shen, L. Yu, N. Feng, and J. Song, A model-predictive-control- based torque demand control approach for parallel hybrid powertrains. IEEE Transactions on Vehicular Technology, 62:1041–1052, 3 2013. ISSN 0018-9545. doi: 10.1109/TVT.2012.2218291.

[5] D. van Mullem, T. Van Keulen, J. Kessels, B. De Jager, M. Steinbuch, Implementation of an optimal control energy management strategy in a hybrid truck. volume 43, 2010. doi: 10.3182/20100712-3-DE-2013.00067.

[6] A. Mayyas, S. Kumar, P. Pisu, J. Rios, P. Jethani, Model-based design validation for advanced energy management strategies for electrified hybrid power trains using innovative vehicle hardware in the loop (vhil) approach. Applied Energy, 204, 2017. ISSN 03062619. doi: 10.1016/j.apenergy.2017.07.028.

[7] P. G. Anselma, Y. Huo, J. Roeleveld, G. Belingardi, A. Emadi, Slope- weighted energy-based rapid control analysis for hybrid electric vehicles. IEEE Transactions on Vehicular Technology, 68, 2019. ISSN 19399359. doi: 10.1109/TVT.2019.2899360.

[8] L. Bruck, A. Emadi, A new regen-based energy management strategy for online control of hybrid powertrains. pages 762–766. IEEE, 6 2021. ISBN 978-1-7281-7583-6. doi: 10.1109/ITEC51675.2021.9490092.

[9] A. Broatch, P. Olmeda, B. Plá, A. Dreif, Novel energy management control strategy for improving efficiency in hybrid powertrains. Energies, 16, 2023. ISSN 19961073. doi: 10.3390/en16010107.

[10] C. Xu, L. Fan, Y. Feng, Y. Zhu, C. Shen, Z. Jiang, A multi-objective optimization energy management strategy for marine hybrid propulsion with waste heat recovery system. Applied Thermal Engineering, 236, 2024. ISSN 13594311. doi: 10.1016/j.applthermaleng.2023.121548.

[11] N. Planakis, G. Papalambrou, N. Kyrtatos, Ship energy management sys- tem development and experimental evaluation utilizing marine loading cycles based on machine learning techniques. Applied Energy, 307, 2022. ISSN 03062619. doi: 10.1016/j.apenergy.2021. 118085.

[12] H. Rezk, A. M. Nassef, M. A. Abdelkareem, A. H. Alami, A. Fathy, Comparison among various energy management strategies for reducing hydrogen consumption in a hybrid fuel cell/supercapacitor/battery system. International Journal of Hydrogen Energy, 46, 2021. ISSN 03603199. doi: 10.1016/j.ijhydene.2019.11.195.

[13] R. Luca, M. Whiteley, T. Neville, P. R. Shearing, D.J.L. Brett, Comparative study of energy management systems for a hybrid fuel cell electric vehicle - a novel mutative fuzzy logic controller to prolong fuel cell lifetime. International Journal of Hydrogen Energy, 47, 2022. ISSN 03603199. doi: 10.1016/j.ijhydene.2022.05.192.

[14] Sailing Innovation Centre. H2c boat. URL: https://www.sailinginnovationcentre.nl/ h2c-boat/.

[15] Torqeedo, Battery and motor technology, URL https://www.torqeedo.com/en/ green-propulsion/battery-technology-com.htmldb40.

[16] O. Tremblay, L. Dessaint, A generic fuel cell model for the simulation of fuel cell vehicles. In 2009 IEEE vehicle power and propulsion conference, pages 1722–1729. IEEE, 2009.

[17] Q. Xun, Y. Liu, J. Zhao, E. A. Grunditz, Modelling and simulation of fuel cel- l/supercapacitor passive hybrid vehicle system. In 2019 IEEE Energy Conversion Congress and Exposition (ECCE), pages 2690–2696. IEEE, 2019.

[18] M. Banaei, M. Rafiei, J. Boudjadar, M. Khooban, A comparative analysis of optimal operation scenarios in hybrid emission-free ferry ships. IEEE Transactions on Transportation Electrification, 6(1):318–333, 2020.

[19] X. Wang, U. Shipurkar, A. Haseltalab, H. Polinder, F. Claeys, R. R. Ne- genborn, Sizing and control of a hybrid ship propulsion system using multi-objective double-layer optimization. IEEE Access, 9:72587–72601, 2021.